SESA 6071

Spacecraft Propulsion

Author: Yusaf Sultan
Lecturer: Charlie Ryan
Word Count: 13659

Contents

List of Weeks

List of Figures

List of Tables

Definitions

$\boldsymbol{I_t}$	Total Impulse (Ns)	$\boldsymbol{I_{sp}}$	Specific Impulse (s)
$\boldsymbol{F}$	Rocket Thrust (N)	$\boldsymbol{g_0}$	Standard Gravitational Accel (m/s^2)
$\boldsymbol{\dot{m}}$	Propellent mass flow rate (kg/s)	$\boldsymbol{m_p}$	Expelled propellent mass (kg)
$\boldsymbol{c}$	Effective exhaust velocity (m/s)	$\boldsymbol{\eta_T}$	Power Conversion Efficiency
$\boldsymbol{P_{in}}$	Input Power (W)	$\boldsymbol{m}$	Spacecraft or launch vehicle mass (kg)
$\boldsymbol{\alpha}$	Specific power plant mass (kg/W)	$\boldsymbol{M_{pow}}$	Power plant mass (kg)
$\boldsymbol{v_e}$	Exhaust velocity (m/s)	$\boldsymbol{P_e}$	Exhaust pressure (Pa)
$\boldsymbol{P_a}$	Atmospheric pressure (Pa)	$\boldsymbol{A_e}$	Exhaust area (m^2)
$\boldsymbol{c^*}$	Characteristic velocity (m/s)	$\boldsymbol{P_c}$	Chamber pressure (Pa)
$\boldsymbol{A_t}$	Throat area (m^2)	**M**	Mass fraction
$\boldsymbol{M_0}$	Initial mass (kg)	$\boldsymbol{M_P}$	Propellent mass (kg)
$\boldsymbol{M_f}$	Fuel mass (kg)	$\boldsymbol{\Delta V}$	Change in velocity (m/s)
$\boldsymbol{\alpha}$	Angle of attack (° or rad)	$\boldsymbol{\delta}$	Gimbal angle (° or rad)
γ	Flight path angle (° or rad)	$\boldsymbol{\theta}$	Pitch angle (° or rad)
$\boldsymbol{D}$	Drag (N)	$\boldsymbol{c_p}$	Specific heat at a constant pressure (J/kgK)
$\boldsymbol{c_v}$	Specific heat at a constant volume (J/kgK)	$\boldsymbol{\theta}$	Pitch angle (° or rad)
$\boldsymbol{D}$	Drag (N)	$\boldsymbol{c_p}$	Specific heat at a constant pressure (J/kgK)
$\boldsymbol{C_F}$	Coefficient of thrust	$\boldsymbol{h}$	Enthalpy (J/ mol)
$\boldsymbol{k}$	Ratio or specific heats		

1. Lecture 1

START OF WEEK 1

1.1. What is Rocket Propulsion ?

Propulsion itself is the **act of changing the motion of a body**, typically by using newtons third law and it can be classified in various types of ways. A more colloquial way of defining rocket propulsion is as **mass drivers**, throwing out mass one way to yield an acceleration in the other.

1.2. Rocket Propulsion Family Tree

In **Figure 1** the rocket propulsion types are grouped by the energy source.

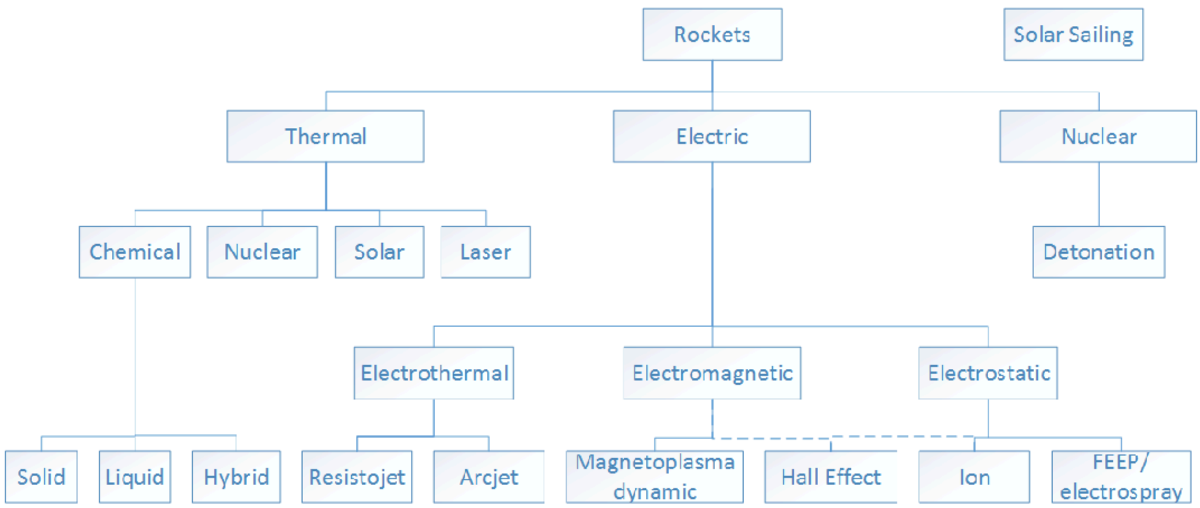

Figure 1: Flowchart of the rocket propulsion family tree

1.2.1. Chemical Rockets

These utilize either a chemical reaction or decomposition to generate energy. Gas is heated to between **700°C - 1300°C** and to speeds between **1.5 km/s - 4.5 km/s**. These require a **fuel and oxidizer** and come in the following types:

- **Solid:** Fuel and oxidizer mixed within into a solid grain which cannot stop burning once ignited. feature **high thrust with low performance**.
- **Liquid:** Burn a liquid fuel and oxidizer allowing for repeated firings and variable thrust. Feature **high performance and thrust with high complexity**.
- **Hybrid:** Have a liquid oxidizer but a solid fuel allowing for better performance than solid with lower complexity.

1.2.2. Electric Rockets

These use electrical energy to generate thrust without utilizing combustion. Typically have very high exhaust velocities (~ **60,000 m/s**) and therefore **very high performance** at the costs of **high complexities and very low thrust**. The four distinct groups are:

- **Electrothermal:** Uses electrical energy to heat a propellent (Resistojet). Are **simple to build** at the cost of **low thrust**.
- **Electrostatic:** Uses electrical energy to accelerate ionized fuel across an electric fields. Feature **good performance** at the cost of **being expensive and low thrust**.
- **Electromagnetic:** Accelerates an ionized fuel using a magnetic field. Fall issue to **low efficiency unless power input is high**.
- **Hall Effect Thruster:** Uses a mixture of both electrostatic and electromagnetic propulsion methods to accelerate propellent. These are the most **commonly used**.

1.2.3. Nuclear Rockets

Broadly speaking there are two types of nuclear rockets, these are:

- **Nuclear Detonation:** Use the shockwave produced when nuclear bombs are detonated to produce thrust (Orion Drive). **High performance and thrust** but are **very dangerous and have limited testing**.
- **Nuclear Thermal:** Uses the heat energy produced during nuclear fission to heat a propellent (typically hydrogen) which is then exhausted. These have **high performance and thrust** but are **dangerous and have limited testing**.

1.2.4. Solar and Laser Rockets

These systems use large diameter telescopes to focus in a laser or solar radiation to heat up a propellent. These systems feature **high theoretical performance and moderate thrust** but are **very complex and lack any real testing**.

1.2.5. Solar Sails

These systems use no propellent at all and instead produce thrust through the momentum gained when a photon is incident on the sail. These systems feature **good performance with no fuel** but fall victim to **low thrust and engineering complexity**.

1.3. Rocket Propulsion Applications

Instead of grouping together rocket propulsion methods using the energy source, the rocket application can also be used, for example:

- **High Thrust/Maneuverability:** Typically have the cost of **low performance** and use **chemical or solid** propulsion methods.
- **High Performance:** Typically have the cost of **low thrust** and use **electrical** propulsion methods.
- **Balanced Thrust and Performance:** Typically the middle ground is **nuclear thermal**.

2. Lecture 2

2.1. Definitions and Fundamentals

To develop a empirical measure of performance we should first consider **Eq. 1**.

$$I_t = \int_0^t F \ \ dt \tag{1}$$

Where:

- $\boldsymbol{I_t}$: Total Impulse (Ns)
- $\boldsymbol{F}$: Thrust Force (N)
- $\boldsymbol{t}$: Burn Duration (s)

Note that for **Eq. 1**, if F is constant then the equation simplified to $I_t = Ft$. A more useful measure of performance for rocket engines is shown in **Eq. 2**.

$$I_{sp} = \frac{\int_0^t F \ \ dt}{g_0 \int_0^t \dot{m} \ \ dt} = \frac{I_t}{g_0 \int_0^t \dot{m} \ \ dt} \tag{2}$$

Where:

- $\boldsymbol{I_{sp}}$: Specific Impulse (s)
- $\boldsymbol{g_0}$: Standard Gravitational Accel (m/s^2) = 9.81 m/s^2
- $\boldsymbol{\dot{m}}$: Propellent mass flow rate (kg/s)

There is no concrete reason on why g_0 is present in this equation, however one common theory is that it allows $I_{sp}$to be in seconds instead of featuring a length unit which would eliminate any error in conversion from metric to imperial. If F and $\dot{m}$ are both constant over the t then **Eq. 2** simplifies to **Eq. 3**.

$$I_{sp} = \frac{I_t}{g_0 m_p} \tag{3}$$

Where:

- $\boldsymbol{m_p}$: Expelled propellent mass (kg) $= \dot{m}t$

Another useful parameter for defining engine performance is shown in **Eq. 4**.

$$c = \frac{F}{\dot{m}} \tag{4}$$

Where:

- $\boldsymbol{c}$: Effective exhaust velocity (m/s)

The exhaust velocity is called as such as the **velocity profile of the exhaust is not uniform**, this is most seen in chemical rockets due to the **no slip condition** but is slightly seen in electrical rockets too. Rearranging all of the previous equations together yields a definition for I_{sp} in terms of c.

$$I_{sp} = \frac{c}{g_0} \tag{5}$$

Typical I_{sp} values for the rocket engine types defined in the previous lecture are shown in **Table 1**.

Rocket Engine Type	$I_{sp}(s)$	Thrust (N)	Efficiency	Propellent
Chemical bi-propellent	200 - 450	$\leq 10MN$	0.8	Liquid or Solid Propellents
Chemical mono-propellent	150 - 250	0.03 - 100	0.9	N_2H_4
Thermal Nuclear Fission	500 - 860	$\leq 10MN$	0.5	H_2
Resistojet - electrothermal	150 - 350	0.01 - 10	0.4	N_2H_4 , NH_3 , H_2
Ion Thruster - electrostatic	1500-8000	$10^{-5} - 0.5$	0.65	Xe
Hall Effect Thruster	1500-2000	$10^{-5} - 2$	0.55	Xe

Table 1: Typical values of I_{sp}

2.2. Maximum Chemical Performance

A typical chemical reaction used in chemical rockets is combustion shown in **Eq. 6**.

$$H_2 + 1/2\ O_2 \longrightarrow H_2O + \text{Energy} \tag{6}$$

Combustion as shown in **Eq. 6** nis an exothermic reaction as the energy of the reactants is more than the energy of the products, allowing for an excess of energy after the reaction. To estimate an effective upper limit to the energy released during combustion, the bond energies shown in **Table 2** can be used.

Chemical	Bond Energy (kJ/mol)
H_2	436
O_2	498
H_2O	428
	498.7

Table 2: Respective bond energies of reactants and products in combustion.

Note that there are two bond energies in **Table 2** due to the OH and the OH - H bonds. The maximum energy can be calculated and are shown in **Figure 2**.

Energy Per Kilogram Released During Combustion

$$M_{Water} := 18.01528\ \frac{gm}{mol} \qquad BE_{H2} := 436\ \frac{kJ}{mol} \qquad BE_{O2} := 498\ \frac{kJ}{mol}$$

$$BE_{OH} := 428\ \frac{kJ}{mol} \qquad BE_{OHH} := 498.7\ \frac{kJ}{mol}$$

$$E_{kg} := \frac{\left(BE_{OH} + BE_{OHH}\right) - \left(BE_{H2} + \frac{BE_{O2}}{2}\right)}{M_{Water}} = 13416388.75\ \frac{J}{kg}$$

Maximum Chemical Performance

$$\eta := 0.9 \qquad g_0 := 9.81\ \frac{m}{s^2}$$

$$c := \sqrt[2]{2\ \eta \cdot E_{kg}} = 4914.21\ \frac{m}{s} \qquad I_{sp} := \frac{c}{g_0} = 500.94\ s$$

Figure 2: Calculations for maximum chemical rocket engine performance

Note that in this calculation, the bond energy of oxygen is halved as per **Eq. 6** and the equation for effective exhaust velocity comes from the kinetic energy equation and noting that $E_{kg} = Energy/mass$.

2.3. Comparative Electric Performance

To compare the efficiency of chemical propulsion to electric propulsion consider an electrostatic propulsion system shown in **Figure 3**.

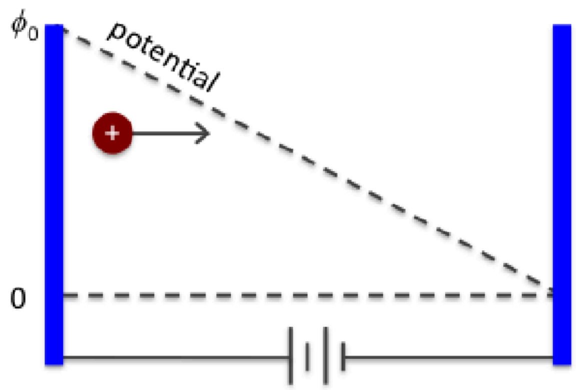

Figure 3: Basic principle of an electrostatic propulsion system.

A charged ion (assumed for these calculations to be a water ion) enters an electric field which causes it be accelerated to the more negative (lower potential plate). By setting the electric potential energy gained by the ion equal to the kinetic energy ($\eta E_p = E_k$) then the I_{sp} can be calculated, shown in **Figure 4**.

Voltage Required for an Isp of 500s Using Ionized Water

$$M_{Water} := 18.01528\ \frac{gm}{mol} \qquad \eta := 0.9 \qquad g_0 := 9.81\ \frac{m}{s^2} \qquad N_a := 6.023 \cdot 10^{23}\ mol^{-1}$$

$$I_{sp} := 500\ s \qquad q := 1.6 \cdot 10^{-19}\ C$$

$$V := \frac{\frac{1}{2} \frac{M_{Water}}{N_a} \left(I_{sp} \cdot g_0\right)^2}{\eta \cdot q} = 2.5\ V$$

Figure 4: Comparative electrical propulsion system voltage calculations.

As shown in **Figure 4** the voltage required to match the performance of a chemical system is very low and easily achievable, in reality electrostatic systems can achieve efficiencies in excess of 10,000s.

2.4. Nuclear Performance

To estimate the performance of a thermal nuclear rocket engine, Uranium-235 fission is considered, where the energy released in one fission event is immediately transferred to a water molecule, this calculation is shown in **Figure 5**.

Energy Transfered to One Water Molecule During One Nuclear Fission Event

$$E_{U235} := 180\ MeV = \left(2.88 \cdot 10^{-11}\right)\ J \qquad M_{Water} := 18.01528\ \frac{gm}{mol} \qquad N_a := 6.023 \cdot 10^{23}\ mol^{-1}$$

$$m_{Water} := \frac{M_{Water}}{N_a} = 0\ kg$$

<- is 2.99x10^-26 but is too small for mathcad to show

$$E_{kg} := \frac{E_{U235}}{m_{Water}} = \left(9.63 \cdot 10^{14}\right)\ \frac{J}{kg}$$

Performance of a Nuclear Thermal System

$$\eta := 0.9 \qquad g_0 := 9.81\ \frac{m}{s^2}$$

$$c := \sqrt[2]{2\ \eta \cdot E_{kg}} = 41631151.15\ \frac{m}{s} \qquad I_{sp} := \frac{c}{g_0} = \left(4.24 \cdot 10^{6}\right)\ s$$

Figure 5: Maximum nuclear thermal propulsive system performance.

Note that this I_{sp} is a theoretical upper limit and in reality the true performance is much lower and is limited by material limits due to heat.

2.5. Definitions and Fundamentals Cont.

For propulsion systems, efficiency can be defined in terms of the fraction of source power that is converted to jet power, this efficiency is shown in **Eq. 7**.

$$\eta_T = \frac{\dot{m}c^2}{2P_{in}} \tag{7.1}$$

$$P_{in} = \frac{\dot{m}c^2}{2\eta_T} = \frac{Fc}{2\eta_T} \tag{7.2}$$

$$\frac{P_{in}}{m} = \frac{F}{m}\frac{c}{2\eta_T} = a\frac{c}{2\eta_T} \tag{7.3}$$

Where:

- $\boldsymbol{\eta_T}$: Power conversion efficiency
- $\boldsymbol{a}$: Acceleration (m/s^2)
- $\boldsymbol{P_{in}}$: Input or Source power (W)
- $\boldsymbol{m}$: Spacecraft mass (kg)

Note that for electrical systems P_{in}, the power must come from a source e.g., solar panel array. **Eq. 7** Also shows that **for a fixed specific power: ($\frac{P_{in}}{m}$) a high effective exhaust speed** (c) **means a low acceleration.** It is also useful to define a specific power plant mass as shown in **Eq. 8**.

$$\alpha = \frac{M_{pow}}{P_{in}} \tag{8}$$

Where:

- $\boldsymbol{\alpha}$: Specific power plant mass (kg/W)
- $\boldsymbol{M_{pow}}$: Power plant mass (kg)

By manipulating equations **Eq. 8** and **Eq. 7**, as well as assuming that $\eta_T \approx 1$ and $M_{pow} \approx 0.1m$ then the acceleration can be written as **Eq. 9**.

$$a = \frac{0.2}{\alpha c} \quad \begin{cases} M_{pow} \approx 0.1m \\ \eta_T \approx 1 \end{cases} \tag{9}$$

Eq. 9 shows that a and c are inversely proportional from one another, meaning a high acceleration will typically mean a low effective exhaust velocity and vice versa. A showing how performance varies with acceleration is shown in **Figure 6**.

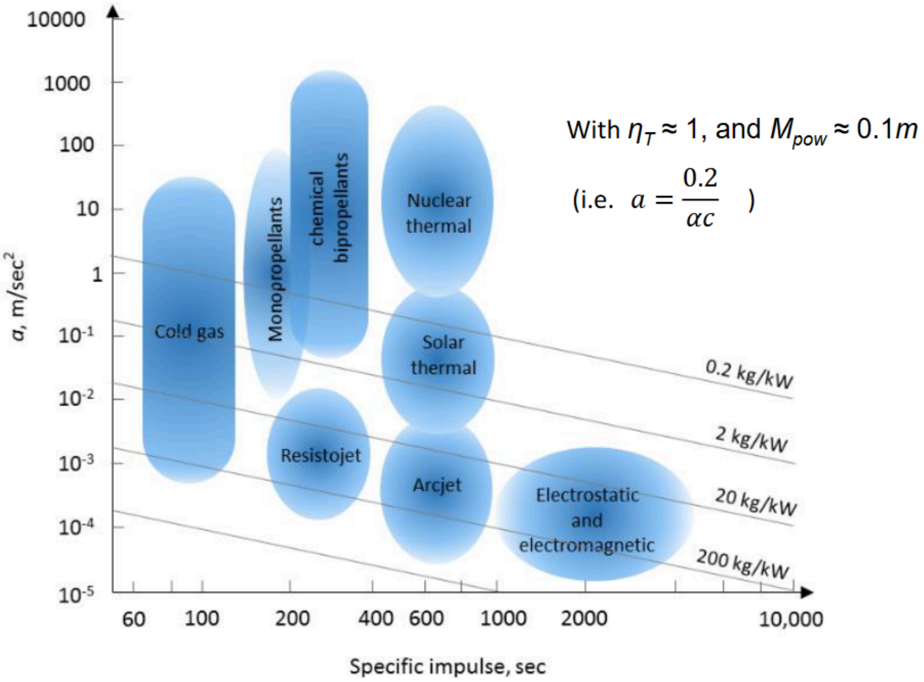

Figure 6: Variation of spacecraft acceleration against performance.

Note that for electrical propulsion systems shown in **Figure 6** a higher I_{sp} means a lower acceleration as $I_{sp} \propto c \propto \frac{1}{a}$. Different power sources have different values of α, for example:

- Nuclear Reactors $\Rightarrow 2kg/kW$
- Solar Panels $\Rightarrow 20kg/kW$
- RTGs $\Rightarrow 200kg/kW$

2.6. Thrust Fundamentals

By apply Newton's second law to a rocket nozzle, considering the difference the atmospheric and exhaust pressure as well as using the equations derived in the previous sections, **Eq. 10** can be derived.

$$F = \dot{m}v_e + (P_e - P_a)A_e \tag{10.1}$$

$$c = v_e + \frac{(P_e - P_a)A_e}{\dot{m}} \tag{10.2}$$

$$I_{sp} = \frac{1}{g_0}\left(v_e + \frac{(P_e - P_a)A_e}{\dot{m}}\right) \tag{10.3}$$

Where:

- $\boldsymbol{v_e}$: Exhaust velocity (m/s)
- $\boldsymbol{A_e}$: Exhaust Area (m^2)
- $\boldsymbol{P_e}$: Exhaust Pressure (Pa)
- $\boldsymbol{P_a}$: Atmospheric Pressure (Pa)

One key thing to note about **Eq. 10** is that the thrust is made up of two parts, the first part being the **momentum thrust** accounting for the majority of the thrust (90-70%) and the second part is the **pressure thrust** (10-30%).

Crucially, as $P_a(h)$ then the I_{sp} and c vary with the height, typically being lower at lower altitudes and increasing up an reaching their maximums in the thinner sections of the atmosphere.

Another impartial performance parameter for chemical rockets which does not depend on the altitude is shown in **Eq. 11**.

$$c^* = \frac{P_c A_t}{\dot{m}} \tag{11}$$

Where:
- $\boldsymbol{c^*}$: Characteristic velocity (m/s)
- $\boldsymbol{P_c}$: Chamber pressure (Pa)
- $\boldsymbol{A_t}$: Throat area (m^2)

Typical values of c^* are 1500 m/s for a solid rocket and 2500 for H_2/O_2 liquid bi-propelled rocket.

2.7. Tsiolkovsy Rocket Equation

One way to represent the quantity of propellent to the structure of the rocket is by using the **propellent mass fraction** shown in **Eq. 12**.

$$\mu = \frac{M_P}{M_0} \tag{12}$$

Where:
- $\boldsymbol{\mu}$: Mass fraction
- $\boldsymbol{M_P}$: Propellent mass (kg)
- $\boldsymbol{M_0}$: Structure Mass (kg)

For a well designed rocket $\mu \approx 0.8 - 0.85$. The famous rocket equation is derived by starting with Newtons second law and considering the momentum of the fuel leaving the engine and integrating that equation, this yields .

$$\Delta V = c \ln\left(\frac{M_0}{M_f}\right) = I_{sp} g_0 \ln\left(\frac{M_0}{M_f}\right) \tag{13}$$

Where:
- $\boldsymbol{\Delta V}$: Change in velocity (m/s)
- $\boldsymbol{M_f}$: Final mass (kg)

The ΔV and the M_0/M_f are plotted against one another in **Figure 7**. Note that for a single stage rocket $M_0/M_f \approx 20$ and the ΔV required to reach LEO is 9.5 km/s and so a single stage to rocket is on the boundary of being possible using a chemical bi-propellent rocket.

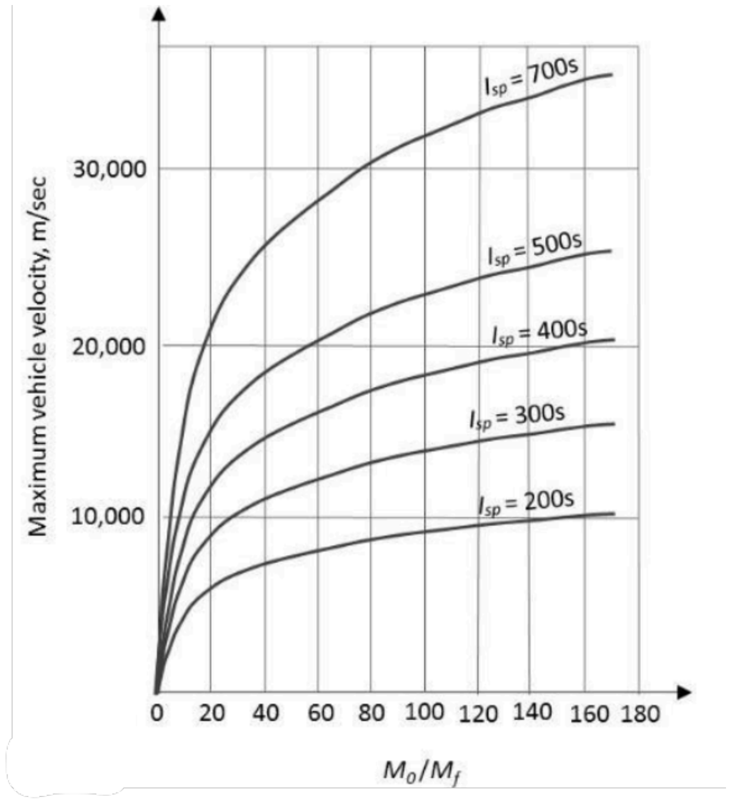

Figure 7: Plot of ΔV against M_0/M_f

3. Lecture 3

3.1. Rocket Staging

The typical ΔVs required for different manoeuvre are shown in **Table 3**.

Manoeuvre	Req ΔV (km/s)
Surface of Earth to LEO (inc drag and grav losses)	9.5
LEO to GEO (impulsive no plane change)	3.95
LEO to GEO (low thrust no plane change)	4.71
LEO to Lunar (impulsive)	3.9
LEO to Lunar (low thrust)	8
LEO to Mars (impulsive)	5.7
GEO station keeping	50 m/s /year
LEO station keeping	< 25 m/s /year

Table 3: Typical ΔV values for different manoeuvre

For a conventional chemical rocket, to reach LEO from the surface of the Earth, assuming an ideal mass ratio ($I_{sp} \approx 450s, \quad \Delta V \approx 9.5km/s, \quad M_o/M_f \approx 8.6$) then the mass fraction μ would have to be $\approx 90\%$, leaving 10% for the payload itself. This is mitigated through using **rocket staging**. Stages offer various benefits, the most prominent of which is the gain in ΔV when compared with one stage. The expression of the ΔV of a multistage rocket is shown in **Eq. 14**.

$$\Delta V_{\text{Total}} = \Delta V_{\text{Stage 1}} + \Delta V_{\text{Stage 2}} + ... + \Delta V_{\text{Stage } n} \tag{14.1}$$

$$\Delta V_{\text{Total}} = I_{sp\ \text{Stage 1}} g_0 \left(\frac{M_{0\ \text{Stage 1}}}{M_{1\ \text{Stage 1}}} \right) \tag{14.2}$$

$$+ I_{sp\ \text{Stage 2}} g_0 \left(\frac{M_{0\ \text{Stage 2}}}{M_{1\ \text{Stage 2}}} \right) \tag{14.3}$$

$$+ ... \tag{14.4}$$

$$+ I_{sp\ \text{Stage } n} g_0 \left(\frac{M_{0\ \text{Stage } n}}{M_{1\ \text{Stage } n}} \right) \tag{14.5}$$

An image depicting the payload fraction against delta V is shown in **Figure 8**.

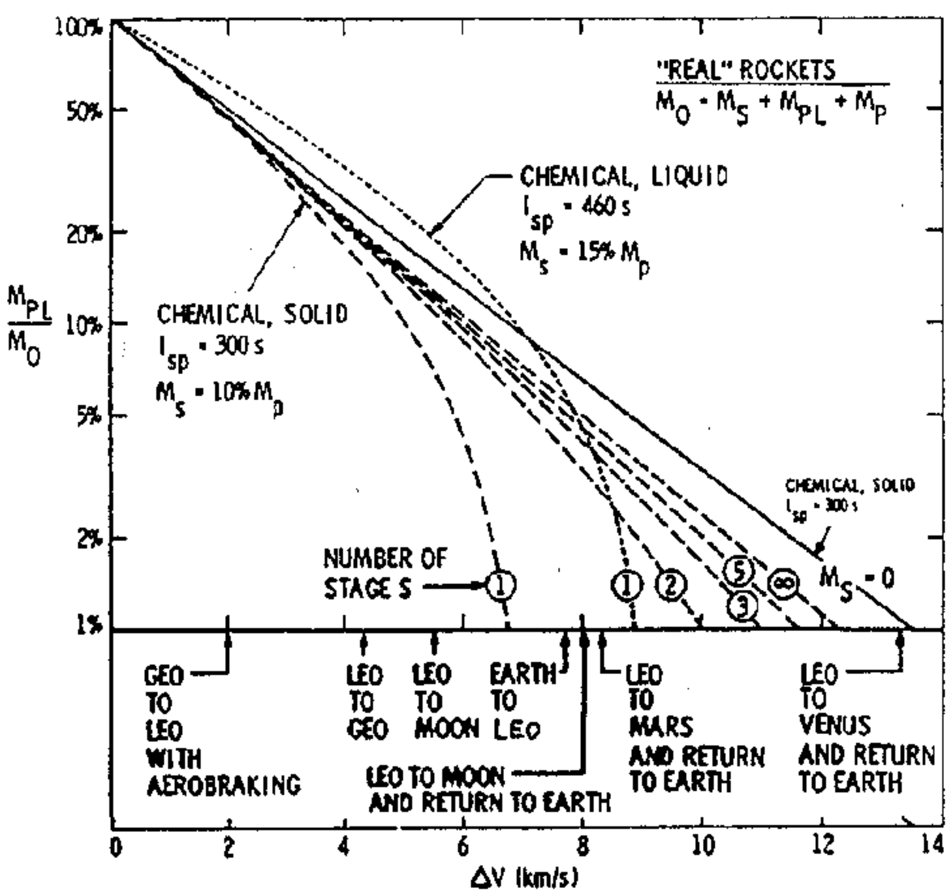

Figure 8: Plot depicting the effect of staging on the ΔV for a given payload fraction.

3.2. Launch Vehicle Dynamics

The key forced acting on a launch vehicle during launch are shown in **Figure 9**.

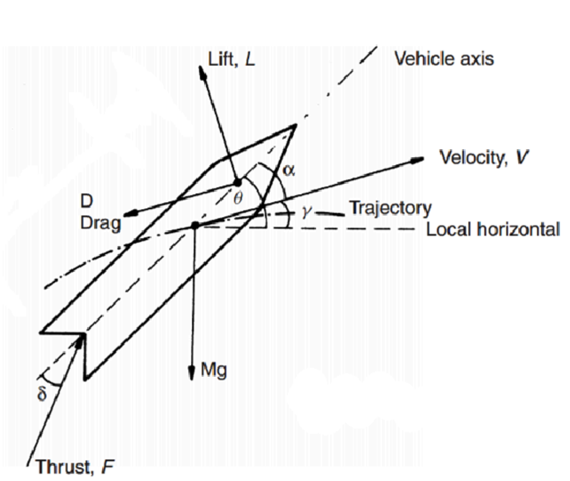

Figure 9: Plot illustrating the forces present on a lunch vehicle.

Taking the forces shown in **Figure 9**, a differential expression can be generated for the motion of the craft, using Newton's second law, this is shown in

$$M\left(\frac{dV}{dt}\right) = F\cos(\alpha - \delta) - Mg\sin(\gamma) - D \tag{15}$$

Where:

- $\boldsymbol{M}$: Total launch vehicle mass (kg)
- $\boldsymbol{F}$: Thrust (N)
- $\boldsymbol{\delta}$: Gimbal angle (° or rad)
- $\boldsymbol{\theta}$: Pitch angle (° or rad) $= \gamma + \alpha$
- $\boldsymbol{V}$: Spacecraft velocity (m/s)
- $\boldsymbol{\alpha}$: Angle of attack (° or rad)
- $\boldsymbol{\gamma}$: Flight path angle (° or rad)
- $\boldsymbol{D}$: Drag (N)

Note that within **Eq. 15**, many of the terms depend on the time as well as on one another. These equations can be rearranged and manipulated to yield **Eq. 16** (assuming $V_0 \approx 0, \alpha \approx 0, \delta \approx 0$).

$$\Delta V = \Delta V_{\text{ideal}} - \Delta V_g - \Delta V_D \tag{16.1}$$

$$\Delta V_{\text{ideal}} = \bar{c}\ln\left(\frac{M_0}{M_f}\right) \tag{16.2}$$

$$\Delta V_g = \int_0^{t_b} g\sin(\gamma)dt \tag{16.3}$$

$$\Delta V_D = \int_0^{t_b} \frac{D/M_0}{1 - \mu t/t_p}dt \tag{16.4}$$

Note that for **Eq. 16**, $\Delta V_g \approx 1.1 km/s, \Delta V_D \approx 0.2 km/s$. Additionally a boost of 0.5 km/s can be gained by launching at the equator. Note that $\bar{c}$ is an averaged effective exhaust velocity.

3.3. Converging Diverging Nozzle

START OF WEEK 2

All of the thermal rockets that were shown in **Figure 1** will most likely use a converging diverging nozzle (De-Laval nozzle) to accelerate the hot exhaust gas and increase the thrust of the engine. They effectively **convert the gases thermal energy to kinetic energy**. Note that when considering gaseous or liquid flow in this module, the following assumptions will be made:

- The fluid used are homogeneous.
- The species are gaseous.
- No heat transfer across the rocket walls (adiabatic assumption).
- No friction and all boundary layer effects effects negligible
- No shock waves or discontinuities in the nozzle
- Gas composition does not change in the noz zle (frozen flow) (not necessarily true but will assume for simplification that all reactions occur in the combustion chamber)

A plot of how the temperature, pressure, velocity and Mach number change over the nozzle is shown in **Figure 10**.

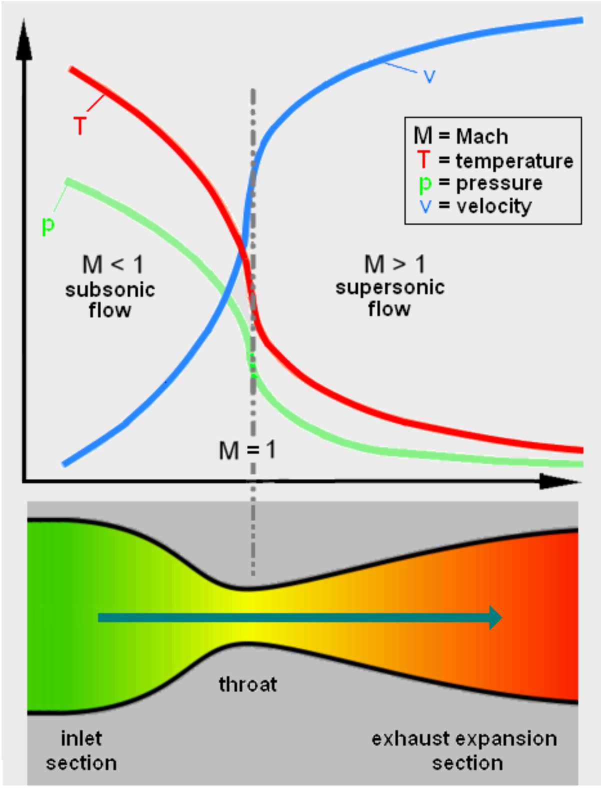

Figure 10: Plot of pressure, temperature, velocity and Mach number over a De-Laval nozzle.

3.4. Exit Velocity Equation

Utilizing the isentropic flow equations it is possible to derive equations for many of the nozzle and engine parameters that have been previously stated. To derive an expression for the **exit velocity** v_e from isentropic flow equations, we first start with the expression for stagnation enthalpy and apply the following criteria shown in **Eq. 17**.

$$h_0 = h_e + \frac{v_e^2}{2} \tag{17.1}$$

$$c_p T_0 = c_p T_e + \frac{v_e^2}{2} \quad \begin{cases} 1. & \text{Ideal gas} \\ 2. & c_p \text{ is constant at a given } T \end{cases} \tag{17.2}$$

Where:

- $\boldsymbol{h_0}$: Stagnation enthalpy (J/mol).
- $\boldsymbol{h_e}$: Enthalpy at nozzle exit (J/mol).
- $\boldsymbol{c_p}$: Specific heat at a constant pressure (J/mol).
- $\boldsymbol{T_0}$: Stagnation temperature (T).
- $\boldsymbol{T_e}$: Temperature at nozzle exit (T).

This equation can be further developed by **assuming isentropic flow** from the stagnation point to the exhaust point. This allows for the isentropic flow equations to apply, which are shown in **Eq. 18**.

$$\frac{T_0}{T_e} = \left(\frac{P_0}{P_e}\right)^{\frac{k-1}{k}} = \left(\frac{\rho_0}{\rho_e}\right)^{k-1} \tag{18}$$

Where:

- $\boldsymbol{P_0}$: Stagnation pressure (pa).
- $\boldsymbol{\rho_0}$: Stagnation density (kg/m^3).
- $\boldsymbol{k}$: Ratio of specific heats.
- $\boldsymbol{P_e}$: Pressure at nozzle exit (pa).
- $\boldsymbol{\rho_e}$: Density at nozzle exit (kg/m^3).

Finally the last equation that is needed for a useful expression for v_e is the equation for the specific heat capacity at a constant pressure c_p, this is shown in **Eq. 19**.

$$c_p = \frac{R}{W}\frac{k}{k-1} \tag{19}$$

Where:

- $\boldsymbol{R}$: Molar gas constant $(J/(\text{mol } K))$.
- $\boldsymbol{W}$: Molecular weight (kg/mol).

Using **Eq. 19**, **Eq. 18** and **Eq. 17**, a useful expression for the exhaust velocity v_e can be derived, this is shown in **Eq. 20**.

$$v_e = \sqrt{\frac{R}{W}\frac{2k}{k-1}T_0\left(1 - \left(\frac{P_e}{P_0}\right)^{\frac{k-1}{k}}\right)} \tag{20}$$

Where T_0, P_0 can be assumed to be the combustion conditions. Alternatively, **Eq. 20** can also be used to define the I_{sp}, shown in **Eq. 21** (**assuming ideal expansion**).

$$I_{sp} = \frac{1}{g_0}\sqrt{\frac{R}{W}\frac{2k}{k-1}T_0\left(1 - \left(\frac{P_e}{P_0}\right)^{\frac{k-1}{k}}\right)} \tag{21}$$

To see what parameters effect the value of v_e and what need sto be maximized, various plots are shown in **Figure 11**.

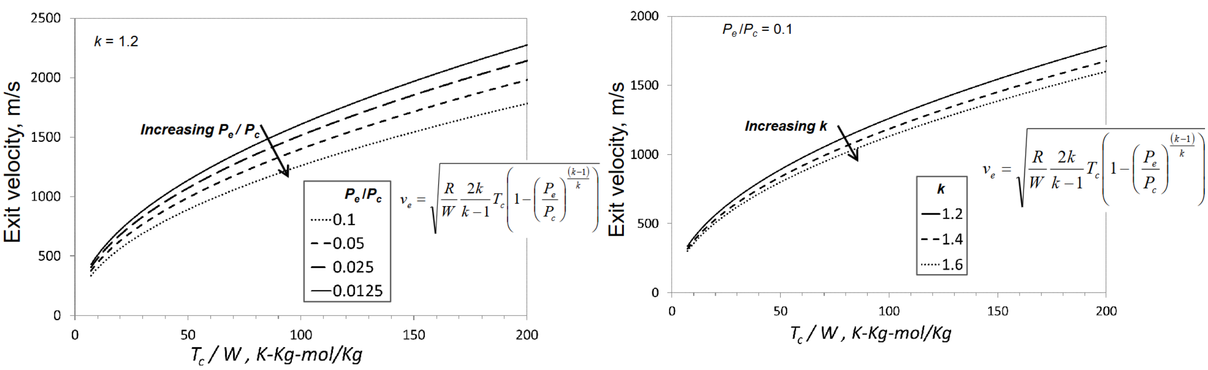

Figure 11: Plot of exit velocity for increasing P_e/P_c ratios [Left], Plot of exit velocity for increasing k ratios [Right]

From **Figure 11** it is clear to see that to maximize the value of v_e the following optimizations of parameters must occur:

- **Minimizing the molecular weight M of the reactants** will have a substantial effect on v_e.

- **Maximizing the combustion temperature** T_c will have a substantial effect on v_e.
- **Decreasing the ratio of** P_e/P_c will have a small impact on v_e.
- **Decreasing the ratio of** k will have a small impact on v_e.

3.5. Mass Flow Rate Equation

Assuming chocked flow (M_a@ Throat ≈ 1), the mass flow rate $\dot{m}$ is given by the expression shown in **Eq. 22**.

$$\dot{m} = \rho_t A_t v_t \tag{22}$$

Where:

- $\boldsymbol{\rho_t}$: Density at the throat (kg/m^3)
- $\boldsymbol{A_t}$: Area of the throat (m^2)
- $\boldsymbol{v_t}$: Velocity at the throat (m/s).

Ideally **Eq. 22** should be expressed in terms of chamber parameters. The first substitution that can be made is an expression for the velocity at the throat v_t using the speed of sound equation, this equation is shown in **Eq. 23**. **Eq. 17** can then be used to yield an expression for the stagnation/chamber pressure, shown again in **Eq. 23**.

$$v_t = a = \sqrt{\frac{kRT_t}{W}} \tag{23.1}$$

$$T_0 = T_t + \frac{v_t^2}{2c_p} = T_t + \frac{\left(M_a\sqrt{\frac{kRT_t}{W}}\right)^2}{2c_p} \tag{23.2}$$

Where:

- $\boldsymbol{a}$: Speed of sound (m/s)
- $\boldsymbol{M_a}$: Mach number

The next goal is to find expressions for the throat temperature and densities as this will then eliminate them from the equation. By using **Eq. 19**, **Eq. 18** and assuming that $M_t \approx 1$ **Eq. 24** can be derived for T_t as well as for ρ_t.

$$T_t = \frac{2T_c}{k+1} \qquad \rho_t = \rho_c\left(\frac{2}{k+1}\right)^{\frac{1}{k-1}} \tag{24}$$

Finally, **Eq. 24** and **Eq. 23** can be substituted into **Eq. 22** to yield **Eq. 25**.

$$\dot{m} = \frac{A_t \rho_c k}{\sqrt{\frac{kRT_c}{W}}}\sqrt{\left(\frac{2}{k+1}\right)^{\frac{k+1}{k-1}}} \tag{25}$$

4. Lecture 4

4.1. Nozzle Expansion Ratio Equation

Momentum conservation can be applied between the exhaust and the throat to yield an expression including A_t and A_e, this expression is shown in **Eq. 26**.

$$\dot{m} = \rho_t A_t v_t = \rho_e A_e v_e \quad \rightarrow \quad \frac{A_t}{A_e} = \frac{\rho_e v_e}{\rho_t v_t} \tag{26}$$

Equations for v_e, v_t and ρ_e/ρ_t have already been defined and so by substituting **Eq. 23**, **Eq. 20** and **Eq. 18** into **Eq. 26** will yield **Eq. 27**.

$$\frac{A_t}{A_e} = \left(\frac{k+1}{2}\right)^{\frac{1}{k-1}} \left(\frac{P_e}{P_c}\right)^{\frac{1}{k}} \sqrt{\frac{k+1}{k-1}\left(1 - \frac{P_e}{P_c}\right)^{\frac{k-1}{k}}} \tag{27}$$

Note that for low altitude rockets $\frac{A_e}{A_t} \approx 3 - 25$ and for high altitude rockets $\frac{A_e}{A_t} \approx 40 - 200$.

4.2. Characteristic Velocity Equation

The characteristic velocity was first defined in **Eq. 11**. It can be rewritten in terms of the equations that have been previously defined to yield **Eq. 28**.

$$c^* = \frac{P_c A_t}{\dot{m}} = \frac{\sqrt{\frac{kRT_c}{W}}}{k\sqrt{\frac{2}{k+1}}^{\frac{k+1}{k-1}}} \tag{28}$$

Note that for a liquid oxygen, liquid hydrogen bipropellant rocket, $c^* \approx 2300 m/s$ and for an ammonium perchlorate + polymer + Al solid rocket, $c^* \approx 1590 m/s$.

4.3. Thrust Equation

Similarly to characteristic velocity, the thrust can be written in terms of the equations that have just been derived, mainly **Eq. 20** and **Eq. 25** to yield **Eq. 29**.

$$F = \dot{m} v_e + (P_e - P_a)A_e = A_t P_c \sqrt{\frac{2k^2}{k-1}\left(\frac{2}{k+1}\right)^{\frac{k+1}{k-1}} \left(1 - \left(\frac{P_e}{P_c}\right)^{\frac{k-1}{k}}\right)} + (P_e - P_a)A_e \tag{29}$$

4.4. Coefficient of Thrust Equation

A useful parameter when quantifying the performance of a nozzle is the coefficient of thrust C_F. The definition of C_F as well as the equation after substituting **Eq. 29** ito it are shown in **Eq. 30**.

$$C_F = \frac{F}{P_c A_t} = \sqrt{\frac{2k^2}{k-1}\left(\frac{2}{k+1}\right)^{\frac{k+1}{k-1}} \left(1 - \left(\frac{P_e}{P_c}\right)^{\frac{k-1}{k}}\right)} + \frac{(P_e - P_a)A_e}{P_c A_t} \tag{30}$$

Values of $C_F \approx 0.8 - 1.9$ with a higher value meaning better thrust amplification. C_F is a peak when there is ideal expansion ($P_e = P_a$) at a constant P_a/P_c. Note that the equation has a **momentum part** and a **pressure part** similar to the thrust itself. The behavior of the C_F against the area and pressure ratios is shown in **Figure 12**

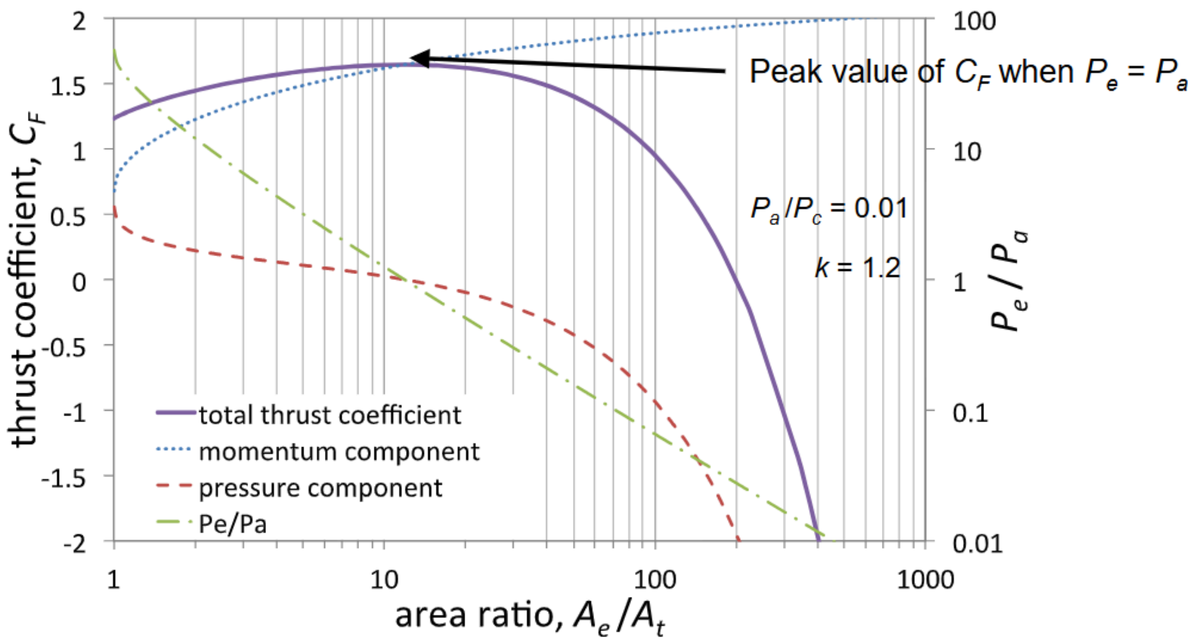

Figure 12: Plot of C_F against area and pressure ratios

Note that as the area ratio increases the momentum component increases but the pressure component decreases. This is interesting as the area ratio **does not appear in the momentum section of the equation**. In reality there is a still a dependency as area ratio depends on pressure ratio which is present in the area ratio equation. Another plot is shown in **Figure 13**.

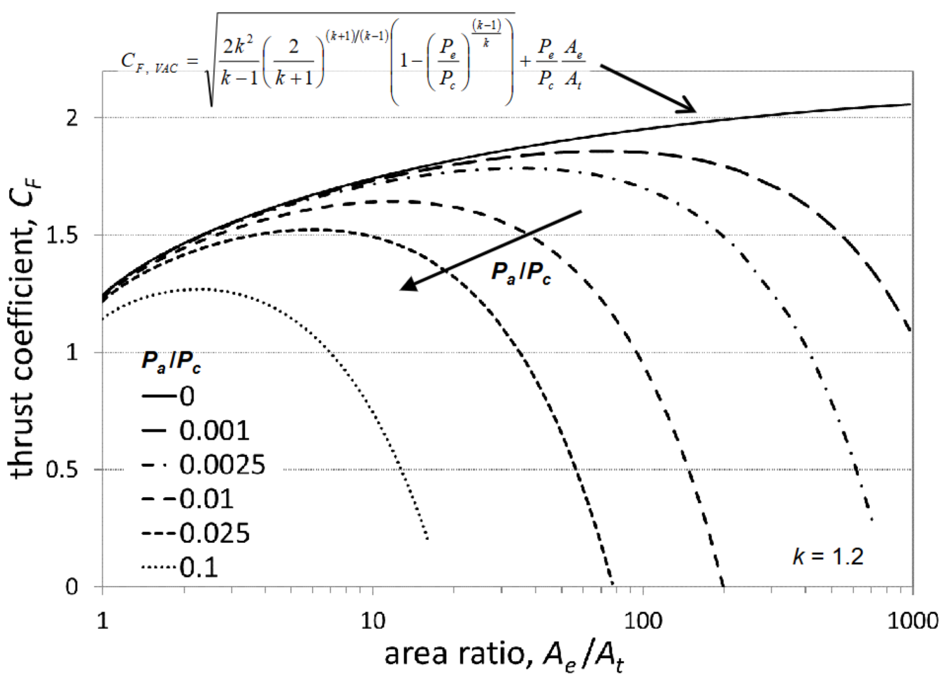

Figure 13: Plot of C_F against area ratio for varying pressure ratios

Note that in **Figure 13**, increasing the pressure ratio will decrease the thrust coefficient. The highest possible thrust coefficient is given when the pressure ratio is zero such as in a vacuum.

4.5. Summary of Equations

$$v_e(R, W, k, T_0, P_e, P_0) = \sqrt{\left(\frac{R}{W}\right)\frac{2k}{k-1}T_0\left(1-\left(\frac{P_e}{P_0}\right)^{\frac{k-1}{k}}\right)} \tag{31.1}$$

$$\dot{m}(A_t, \rho_c, k, R, T_c, W) = \frac{A_t \rho_c k}{\sqrt{\frac{kRT_c}{W}}}\sqrt{\left(\frac{2}{k+1}\right)^{\frac{k+1}{k-1}}} \tag{31.2}$$

$$\frac{A_t}{A_e}(k, P_e, P_c) = \left(\frac{k+1}{2}\right)^{\frac{1}{k-1}}\left(\frac{P_e}{P_c}\right)^{\frac{1}{k}}\sqrt{\frac{k+1}{k-1}\left(1-\left(\frac{P_e}{P_c}\right)^{\frac{k-1}{k}}\right)} \tag{31.3}$$

$$c^*(T_c, k, R, W) = \frac{\sqrt{\frac{kRT_c}{W}}}{k\sqrt{\left(\frac{2}{k+1}\right)^{\frac{k+1}{k-1}}}} \tag{31.4}$$

$$F(A_t, P_c, k, P_e, A_e, P_a) = A_t P_c \sqrt{\frac{2k^2}{k-1}\left(\frac{2}{k+1}\right)^{\frac{k+1}{k-1}}\left(1-\left(\frac{P_e}{P_c}\right)^{\frac{k-1}{k}}\right)} + (P_e - P_a)A_e \tag{31.5}$$

$$C_{F(k,P_e,P_a,A_e,P_c,A_t)} = \sqrt{\frac{2k^2}{k-1}\left(\frac{2}{k+1}\right)^{\frac{k+1}{k-1}}\left(1-\left(\frac{P_e}{P_c}\right)^{\frac{k-1}{k}}\right)} + \frac{(P_e - P_a)A_e}{P_c A_t} \tag{31.6}$$

4.6. Equations Involving Mach Relations

Many of the previous equations can be represented in terms of mach number, namely **Eq. 18**, which are shown in **Eq. 32**.

$$T_0 = T\left(1+\frac{1}{2}(k-1)M^2\right) \quad P_0 = P\left(1+\frac{1}{2}(k-1)M^2\right)^{\frac{k}{k-1}} \quad \rho_0 = \rho\left(1+\frac{1}{2}(k-1)M^2\right)^{\frac{1}{k-1}} \tag{32}$$

The Mach relations can be applied to **Eq. 27** to yield an expression fr the area ratio in terms of Mach number shown in **Eq. 33**.

$$\frac{A_y}{A_x} = \frac{M_x}{M_y}\sqrt{\left(\frac{1+\frac{1}{2}(k-1)M_y^2}{1+\frac{1}{2}(k-1)M_x^2}\right)^{\frac{k+1}{k-1}}} \tag{33}$$

Eq. 33 shows that area ratio is directly proportional top the Mach ratio. Furthermore this equation is also proportional to coefficient of thrust as was previously states, and this relation is also shown in **Figure 14**.

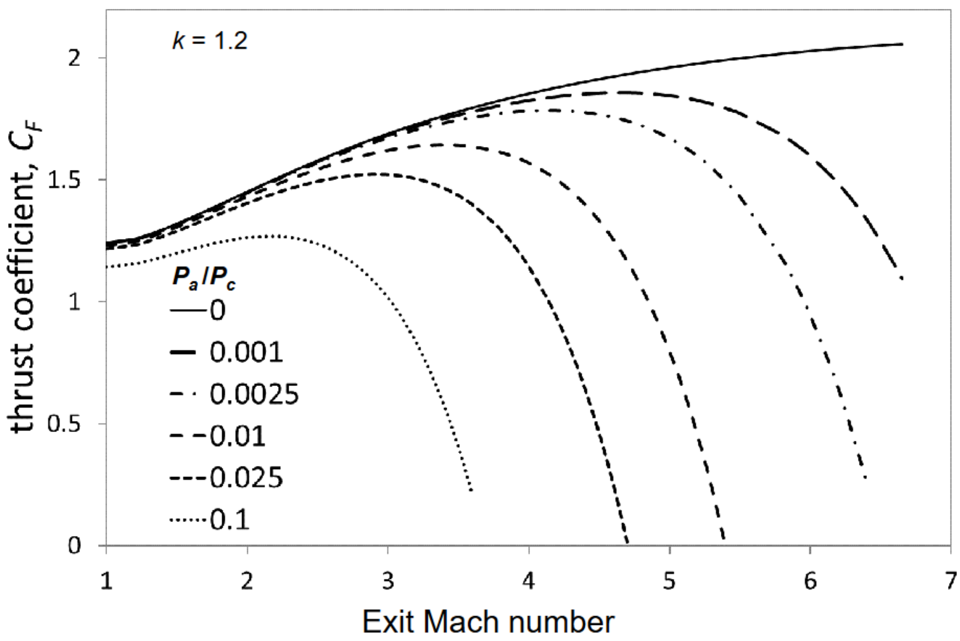

Figure 14: Plot of C_F against exit Mach number for varying pressure ratios

Figure 14 is effectively the same as **Figure 13** apart from altering the x-axis. A larger mach number will require a larger area ratio which will drive up the C_F as it depends on the pressure ratio which is proportional.

4.7. Coefficient of Thrust for Converging Nozzles

Figure 14 can be further edited to yield a neater plot. To get to this, consider the pressure equation in **Eq. 32** when there is no diverging nozzle. This would mean that $M_e = 1$ and **Eq. 32** can therefore be then written as **Eq. 34**.

$$\frac{P_c}{P_e} = \left(1 + \frac{1}{2}(k-1)M_e^2\right)^{\frac{k}{k-1}} \quad \text{If } M_e = 1 \rightarrow \quad \frac{P_e}{P_c} = \left(\frac{2}{k+1}\right)^{\frac{k}{k-1}} \tag{34}$$

Eq. 34 can be substituted into **Eq. 30** to yield an equation for C_F for the converging section of the nozzle, this is shown in **Eq. 35**.

$$C_{F\ \text{Converging}} = (k+1)\left(\frac{2}{k+1}\right)^{\frac{k}{k-1}} - \frac{P_a}{P_c} \tag{35}$$

Using **Eq. 35** a modified version of **Figure 14** can be plotted, this plot is shown in **Figure 15**. This plot now has a point where all lines roginiate, when the ratio of $C_F/C_{F\ \text{Converging}} = 1$ and $A_e/A_t = 1$ when there is no diverging section at all.

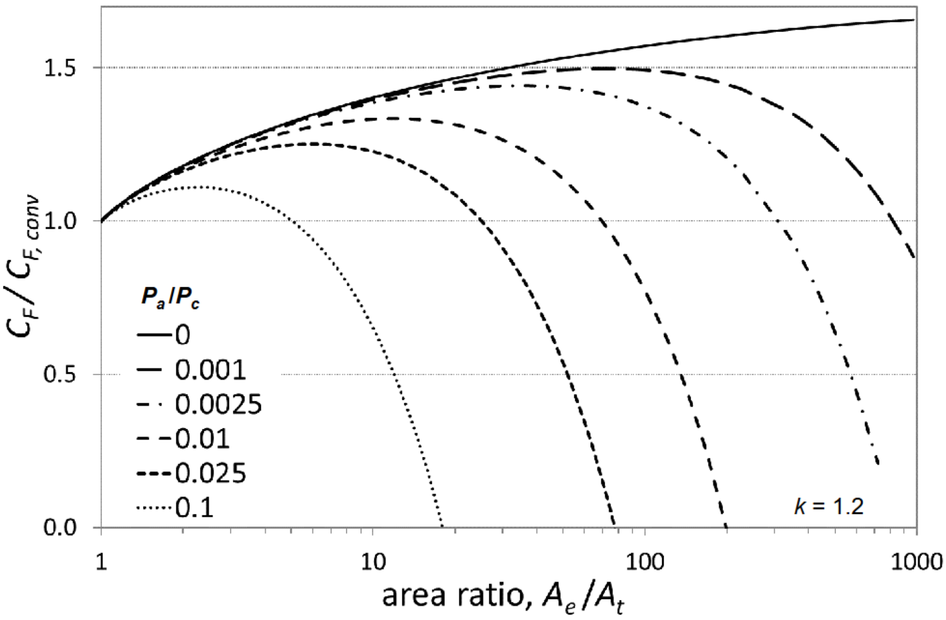

Figure 15: Plot of $C_F/C_{F\text{ Converging}}$ against exit area ratio for varying pressure ratios

4.8. Under, Ideal and Over Expanded Nozzles

Depending on the relationship between the exit pressure P_e and the ambient pressure P_a, there are three cases of nozzle exhaust flow, these are:

- **Under-expanded** ($P_e > P_a$):
  - Typically occurs at **high altitudes** and happens when the **nozzle is too short** .Exhaust wasn't expanded enough and so expands out the back of the nozzle via expansion waves.
  - C_F and thrust are **below maximum**.

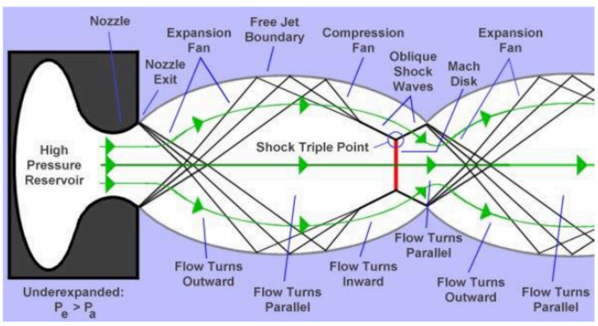

Figure 16: Under-expanded flow out of a nozzle

- **Ideally Expanded** ($P_e \approx P_a$):
  - **Nozzle is perfect length** and exhaust exits in a perfect rectangular plume with no losses or shocks.
  - C_F and thrust are **maximized**.
  - $v_e = c$, exhaust velocity is equal to effective exhaust velocity.

- **Over-expanded** ($P_e < P_a$):
  - Typically occurs at **low altitudes** and happens when the **nozzle is too long**. Exhaust is at a lower pressure than ambient causing shocks and possible flow separation within the nozzle.
  - C_F and thrust are **below maximum**.

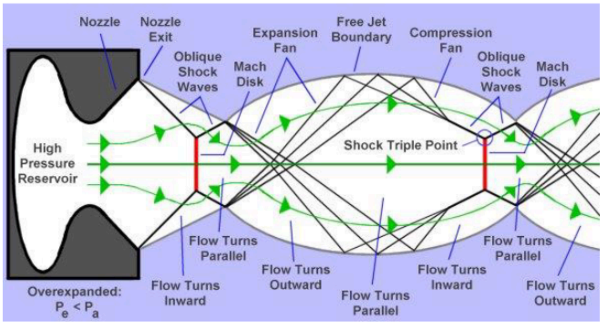

Figure 17: Over-expanded flow out of a nozzle

Plotting the behavior of the thrust coefficient against pressure ratio and the area ratio yields **Figure 18**. Note that the value of C_F is maximized when $P_e = P_a$ and $P_e/P_a = 1$.

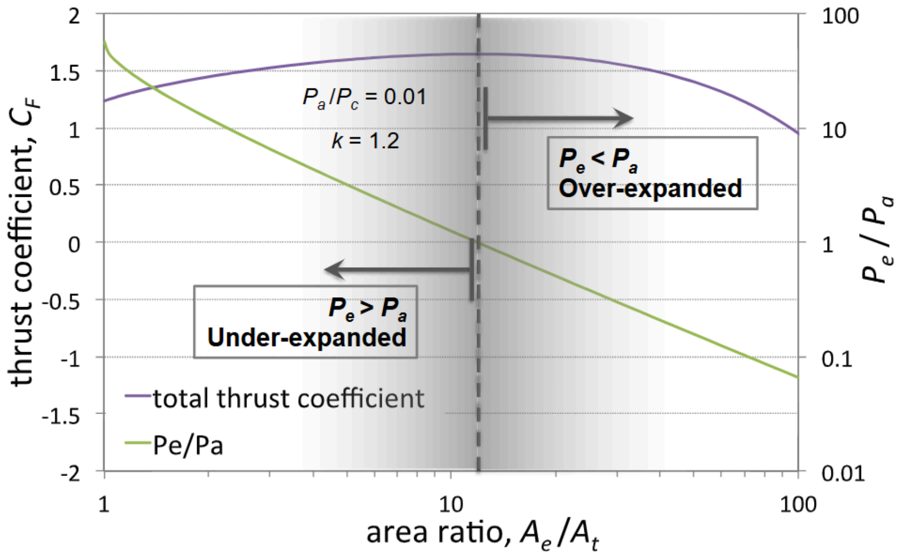

Figure 18: Plot of C_F against pressure ratio and area ratio

4.8.1. Summerfield Criterion

The Summerfield criterion applies to heavily over-expanded nozzles and describes when the flow is likely to separate from inside of the nozzle and create shocks. The criterion is shown in **Eq. 36**.

$$P_e < (0.25 \text{ to } 0.4) P_a \tag{36}$$

Eq. 36 as well as the line of ideal expansion can be applied to **Figure 15** to produce **Figure 19**.

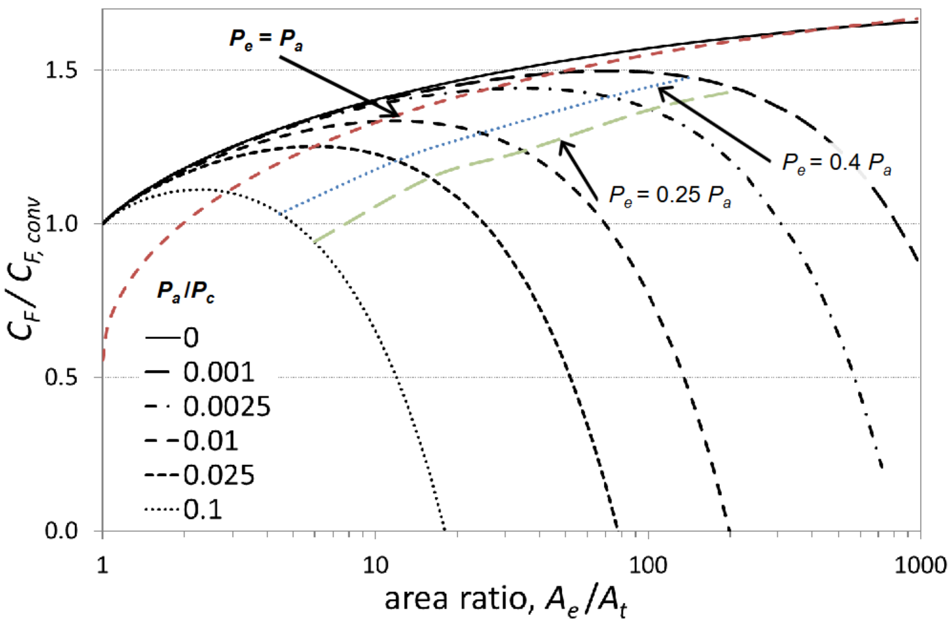

Figure 19: Plot of $C_F/C_{F\ \text{Converging}}$ against exit area ratio for varying pressure ratios with summerfield criterion and ideal expansion line.

On **Figure 19**, the red dotted line represents ideal expansion. **Below this line** sits **over-expanded flow**. **Above this line** sits **under-expanded flow**. **Below the yellow and blue lines** sits **super over-expansion** when the Summerfield criterion applies. Note that a typical rocket fired at sea level will undergo the following movements through this graph:

1. Initially **over-expanded** at sea level.
2. As the altitudes rises the rocket engine moves vertically upwards on the graph and the engine becomes less and less over-expanded until it is **ideally-expanded**.
3. As the rocket ascends further, the engine starts to become **under-expanded** and thrust and C_F start to decrease.

5. Lecture 5

5.1. Nozzle Designs and the Perfect Nozzle

Ideally a nozzles expansion ratio A_e/A_t should increase as the rocket increases in altitude so that the flow is constantly ideally expanded. Some rockets achieve this using a skirt which drops down at higher altitudes to increase A_e/A_t. Some nozzle designs are shown in **Figure 20**

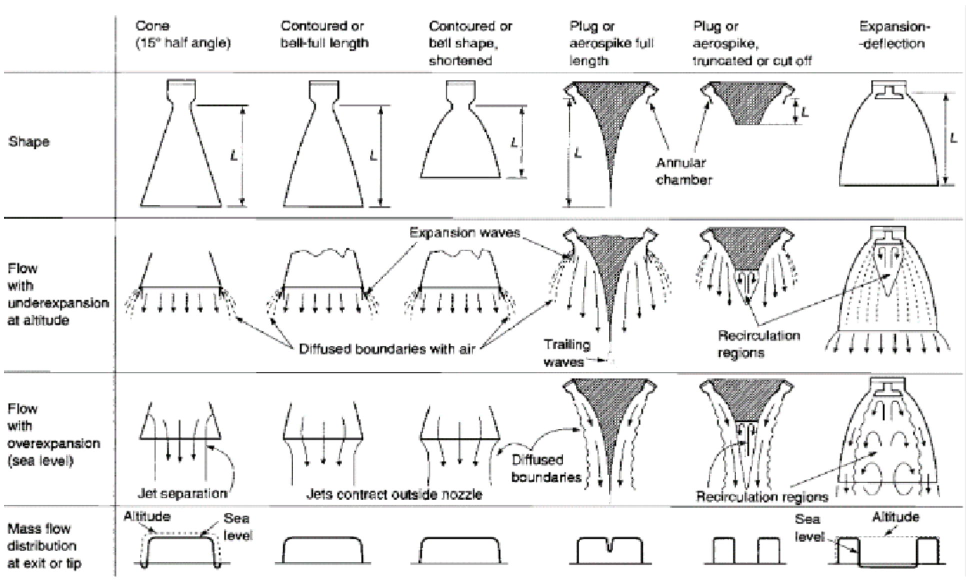

Figure 20: Various nozzle designs.

5.2. Conical Nozzles

Conical nozzles are a relatively simple nozzle design that is also easy to manufacture. There are various parameters that control, the shape of a conical nozzle, these are depicted within **Figure 21**.

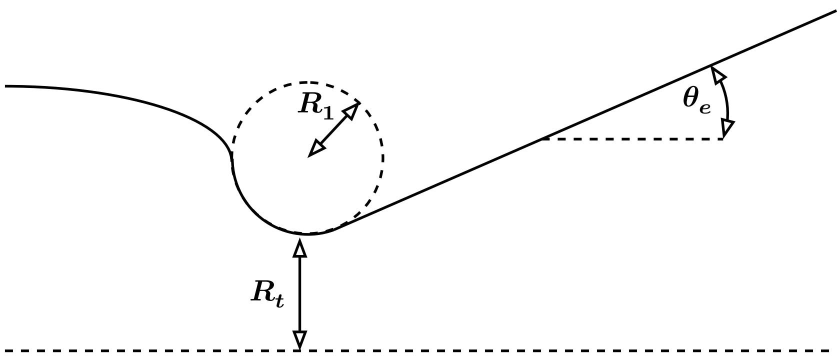

Figure 21: Definitions for a conical nozzle

Where:
- $\boldsymbol{R_t}$: Throat radius (m).
- $\boldsymbol{R_1}$: Throat radius of curvature (m) $\approx 1.5 \times R_t$
- $\boldsymbol{\theta_e}$: Cone divergence half angle (° or Rad)

Ideally $\theta_e \approx 12° - 18°$ with:

- **Smaller angles** constituting a larger I_{sp} but higher mass and more complexity
- **Larger angles** constituting a lower I_{sp} but lower mass.

One issue with conical nozzles is that the flow does not all go directly straight out of the nozzle, it is instead directed outwards slightly at the edges. This introduces losses which are characterized by **Eq. 37** and are only applied to the **momentum term**. This is then applied to C_F.

$$\lambda = \frac{1}{2}(1 + \cos\theta_e) \tag{37.1}$$

$$C_{F(\lambda,k,P_e,P_a,A_e,P_c,A_t)} = \lambda\sqrt{\frac{2k^2}{k-1}\left(\frac{2}{k+1}\right)^{\frac{k+1}{k-1}}\left(1-\left(\frac{P_e}{P_c}\right)^{\frac{k-1}{k}}\right)} + \frac{(P_e - P_a)A_e}{P_c A_t} \tag{37.2}$$

5.3. Bell (Rao) Nozzles

Bell nozzles have typically higher efficiency than conical by allowing the flow to quickly expand whilst it has high pressure and then slowly redirecting the flow to be as axial as possible by the end. An image showing the key dimensions for a bell nozzle are shown in.

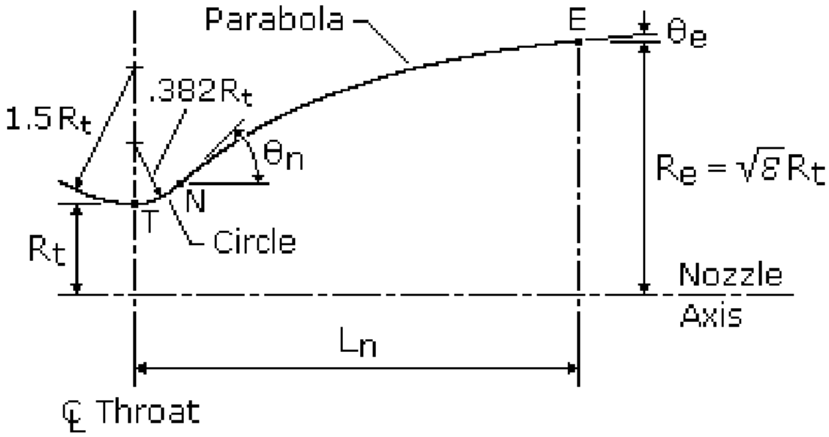

Figure 22: Bell nozzle dimensions.

Note that the bell curve will have a **point of inflection** along it. The coordinates of the inflection point are given by **Eq. 38** the following coordinates relative to the center of the throat (where R_t is measured from).

$$X_n = R_t \sin\theta_N \qquad Y_n = R_t + R_1(1 - \cos\theta_e) \tag{38}$$

Note that θ_N here is the angle that the line at the inflection point makes with the horizontal datum (initial large divergence angle). If the initial diverging section of the nozzle is conical then this would be the cone angle for that portion. The equation for the parabolic low divergence angle section is shown in **Eq. 39**.

$$y' = Px' + Q + (Sx' + T)^{0.5} \tag{39.1}$$

$$P = \frac{y'_E \tan\theta_N + y'_E \tan\theta_E - 2x'_E \tan\theta_E \tan\theta_N}{2y'_E - x'_E \tan\theta_M - x'_E \tan\theta_E} \qquad S = \frac{(y'_E - Px'_E)^2(\tan\theta_N - P)}{x'_E \tan\theta_N - y'_E} \tag{39.2}$$

$$Q = \frac{S}{2(\tan\theta_N - P)} \quad T = Q^2 \tag{39.3}$$

Note that in **Eq. 39** any terms with a subscript of E are the coordinates and angles relating to the exit of the nozzle and the coordinates themselves are relative to the inflection point. Typically $\theta_E \approx 2° - 8°$. The length of a bell nozzle is compared to a 15° conical nozzle using **Eq. 40**.

$$L_{15} = \eta_{\text{Bell}} \frac{R_T(\sqrt{\varepsilon} - 1) + R_1\left(\frac{1}{\cos\theta_e} - 1\right)}{\tan\theta_e} \tag{40}$$

Where:

- $\boldsymbol{L_{15}}$: Length of a 15 ° conical nozzle (m).
- ε: Expansion ratio = A_e/A_t
- $\boldsymbol{\theta_e}$: Divergence angle at exit (° or Rad)
- $\boldsymbol{\eta_{\text{Bell}}}$: Percentage of full bell.

To obtain an values for θ_E, θ_N and ε for a given value of η_{Bell} then **Figure 23** can be used.

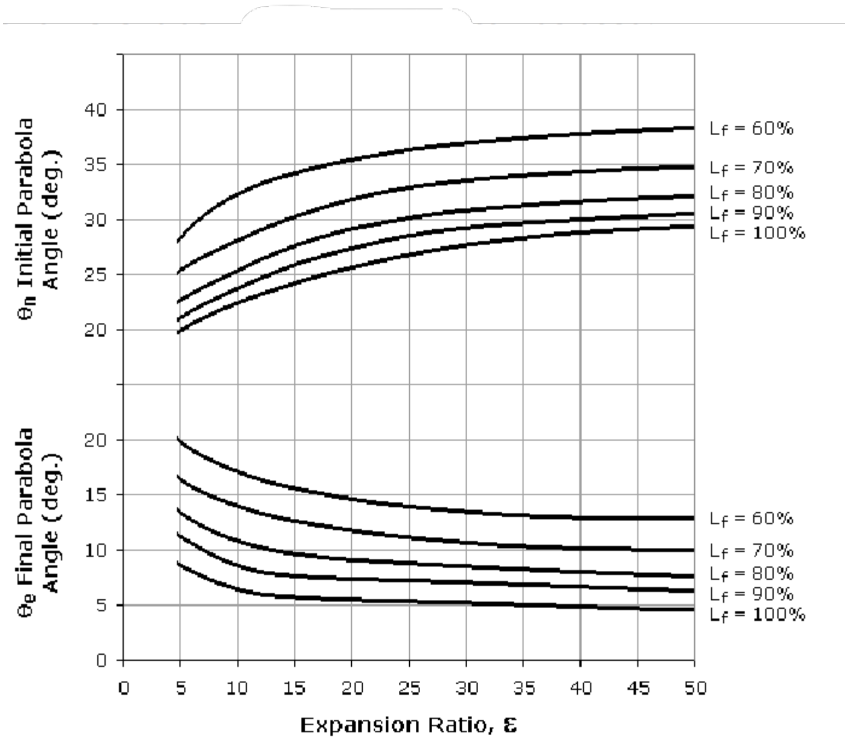

Figure 23: Bell curves for various values of η_{Bell}.

5.4. Aerospike Nozzles

Aerospike nozzles are a version of altitude compensating engine where the external air pressure changes the value of $A_{e\text{ Effective}}$ as it rises in altitude. They commonly feature many smaller combustion chambers which then have their exhausts directed onto a spike. The two main types of aerospike engines (shown in **Figure 20**) are:

- **Full Aerospike**: Feature a full length spike where there is no recirculation region, however the end of the spike is typically difficult to cool.

- **Truncated Aerospike**: The end of the spike is missing which allows for better cooling at penalty of lower performance.

Aerospikes can come in linear and annular forms. They are typically smaller than typical bell nozzles and can still vector thrust by controlling the thrust coming from individual combustion chambers. They haven't yet had much proven flight experience and lack any larger surface area examples.

5.5. Expansion Deflection Nozzle

Make use of a pintle at the center of the nozzle which redirects the flow along the walls of the nozzle (again shown in **Figure 20**). At low altitudes a large recirculation area caused by the high ambient pressure causes a smaller value of A_e. At higher altitudes the lower ambient pressure means the recirculation area is much smaller and the value of A_e is bigger. These engines haven't seen much use with one issue being keeping the pintle itself cool.

5.6. Intro to Liquid Propulsion

START OF WEEK 3

There are three main sub categories within liquid propulsion, these are shown in the bullet pointed list below. The relative performance of these liquid propulsion methods is shown in **Table 4**:

Type	$I_{sp}(s)$	$T_{max}(°C)$	Thrust (N)	Propellants
Monopropellant	200 - 250	600 - 800	0.03 - 100	N_2H_4, H_2O_2
Bipropellant	200 - 468	2500 - 4100	$\leq$ 10 MN	N_2H_4, H_2, Kerosene, N_2O_4
Cold Gas	50 - 100	N/A	0.01 - 270	He, H_2, Kr, N_2

Table 4: Typical liquid propellent parameters.

- **Bipropellant**: Mix together a liquid fuel and liquid oxidizer and combust them to produce thrust.

- **Monopropellent**: Flow a liquid fuel over a catalyst bed where it undergoes a exothermic decomposition reaction.

- **Cold Gas**: A gas is stored at pressure where it is released and flows through a nozzle to accelerate it.

From **Eq. 20**, a good rocket engine will maximize and minimize the following parameters:

- **Low molecular weight** of **combustion products** W. This is also why typically rocket engines operate fuel rich as the low molecular weight fuel dominates the reaction.

- **High combustion temperature** T_c.

- **High combustion pressure** P_c, though there is a smaller gain from this parameter.

- **Low ratio of specific heats** k, though there is a smaller gain from this parameter. Typically k sits at about one anyways.

6. Lecture 6

6.1. Performance of Liquid Thrusters

There are many engine parameters which can be calculated using the equations in **Eq. 31**, however there are many parameters, mainly the combustion parameters (W and k) which cannot be calculated as easily. A **chemical reaction simulator** such as NASA's Glenn Chemical Equilibrium with Applications simulator can be used (***Press to go to link***). One useful parameter is the **oxidizer to fuel ratio**, shown in **Eq. 41**.

$$r = \frac{\dot{m}_{\text{ox}}}{\dot{m}_{\text{fuel}}} \tag{41}$$

Typically, rocket engines **burn fuel rich** and not purely stoichiometric. This is to decrease W as lighter molecules make up more of the exhaust. An example of this is shown in **Figure 24**.

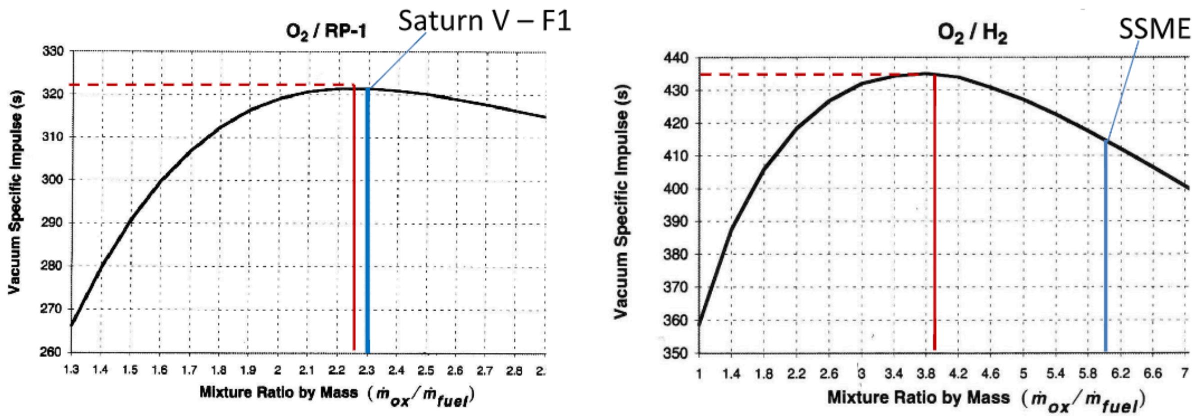

Figure 24: $\dot{m}_{\text{ox}}/\dot{m}_{\text{fuel}}$ against I_{sp} for different rocket engines.

Note that the stoichiometric ratio for r for the Saturn V F1 engines was 3.4 and for the Space Shuttle Main Engines (SSME) it was 8. Note that the Space shuttle couldn't reach r_{optimum} due to the low density of hydrogen and the lack of anymore space in the main fuel tanks for any more fuel.

6.2. Fuels

Name	Chemical Formula	Chemical Structure	Type	Toxicity	Corrosivity	Flammability	Hypergolic?	Molecular Weight (g/mol)	Density (kg/m^3)	Boiling and Freezing Temp ($°C$)
Fuels										
Liquid Hydrogen (LH2)	H_2	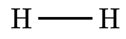	Bi	None	None	High	No	2.016	70.85	Boil: -253 Freeze: -259
RP-1 (Rocket Propellent Group 1)	$C_nH_{1.97n}$	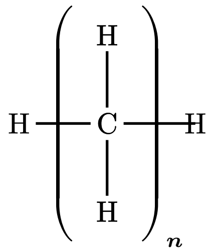	Bi	Moderate	None	High	No	170	810	Boil: 277 Freeze: -40
Hydrazine	N_2H_4	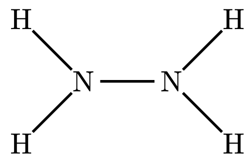	Mono	High	Moderate	Spontaneous	N/A	32.05	1021	Boil: 113.5 Freeze: 2
Monomethylhydrazine (MMH)	CH_3NHNH_2	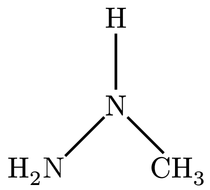	Bi	High	High	High	Yes	46.07	880	Boil: 87.5 Freeze: -52.4
Unsymmetrical Dimethylhydrazine (UDMH)	$(CH_3)_2NNH_2$	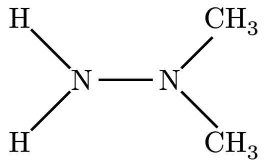	Bi	High	High	High	Yes	60.1	793	Boil: 63 Freeze: -58
Methane	C_2H_4	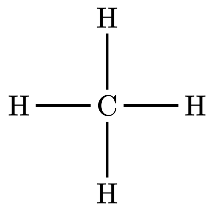	Bi	None	None	High	No	16.04	422.6	Boil: -162 Freeze: -183
Ethanol	C_2H_5OH	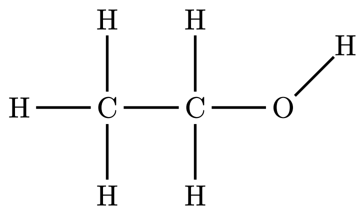	Bi	High	Moderate	High	No	46.07	789	Boil: 78.37 Freeze: -114
Pentaborane	B_5H_9	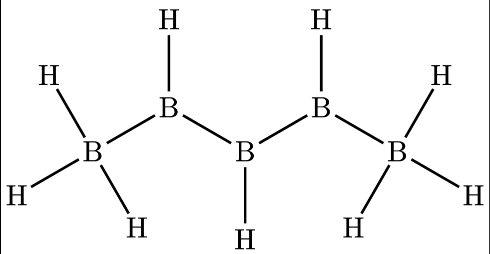	Bi	Extremely	Extremely	Pyrophoric	Yes	63.13	618	Boil: 58.4 Freeze: -46.8

Name	Chemical Formula	Chemical Structure	Type	Toxicity	Corrosivity	Flammability	Hypergolic?	Molecular Weight (g/mol)	Density (kg/m^3)	Boiling and Freezing Temp ($°C$)
Oxidizers										
Liquid Oxygen (LOX)	O_2	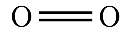	Bi	None	None	N/A	No	32	1141	Boil: -182 Freeze: -218
Dinitrogen Tetroxide	N_2O_4	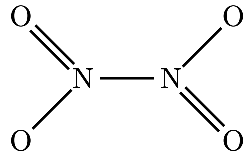	Bi	Extremely	High	N/A	Yes	92.01	1440	Boil: 21.2 Freeze: -11.2
Hydrogen Peroxide	H_2O_2	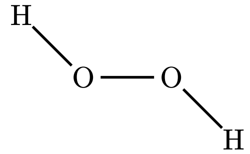	Bi	High	High	N/A	No	34.014	1450	Boil: 150.2 Freeze: -0.43
Nitric Acid	HNO_3	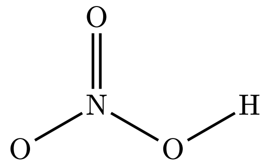	Bi	High	High	N/A	No	63.012	1510	Boil: 83 Freeze: -42
Chlorine Trifluoride	ClF_3	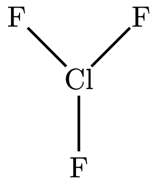	Bi	Extreme	Extreme	N/A	Yes	92.45	1800	Boil: 11.75 Freeze: -76.34
Oxygen Diflouride	OF_2	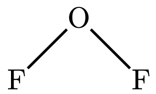	Bi	Extreme	Extreme	N/A	No	54	1880	Boil: -144.75 Freeze: -223.8
Flourine	F_2	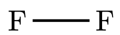	Bi	Extreme	Extreme	N/A	Yes	38	1513	Boil: -188.1 Freeze: -219.6

Table 5: Data on common liquid fuels and oxidizers

Note that nitrogen textoroxide shown in **Table 5** is usually mixed with nitric oxide NO to increase the temperature range over which it is liquid, this mixture is called **Mixed Oxides of Nitrogen** (MON). To compare different fuel and oxidizer ratios, **Table 6** can be used.

Oxidizer	Fuel	Mass Mixture Ratio	ρ (g/cm^3)	c^* (m/s)	Sea Level I_{sp} (s)
O_2	Methane	3.20	0.81	1.84	296
	Hydrazine	0.74	1.06	1.87	301
	Hydrogen	3.40	0.26	2.43	386
	RP-1	2.24	1.01	1.77	300
	UDMH	1.39	0.96	1.84	295
F_2	Hydrazine	2.30	1.31	2.21	365
	Hydrogen	4.54	0.33	2.53	389
N_2O_4	Hydrazine	1.08	1.20	1.77	283
	RP-1	3.4	1.23		297
	MMH	1.65	1.16	1.59	278
H_2O_2	RP-1	7.0	1.29		297

Table 6: Performance parameters for different fuel and oxidizer combinations.

One new area of interest is **green hypergolic fuels** such as Dimethylthioformamide. These are safer and more environmentally friendly alternatives to traditional rocket fuels.

6.3. Overview of Monopropellant Thruster Systems

These systems generate thrust by flowing a propellent over/through a catalyst bed, where it endothermically decomposes, generating a hot, high velocity exhaust gas. The performance of such systems is shown in **Table 4** with a top level systems drawing of a thruster shown in **Figure 25**.

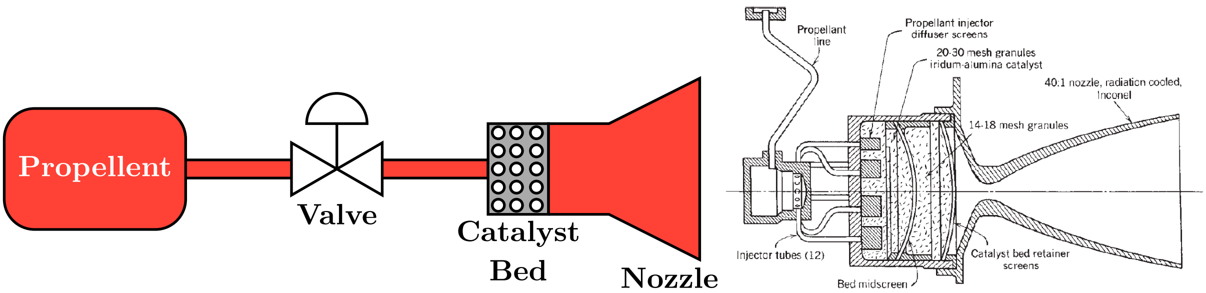

Figure 25: System engineering diagram of a monopropellant thruster system [Left], real schematic of a monopropellant thruster [Right]

6.3.1. Decomposition of Hydrazine

Hydrazine is the most common monopropellent fuel used in rockets. It decomposes over a catalyst bed following the reaction detailed in **Figure 26**.

$$N_2H_4 \longrightarrow 4/3\ NH_3 + 1/3 N_2 + \text{Energy}$$

Figure 26: Decomposition reaction of hydrazine.

This exothermic decomposition reaction has a equilibrium temperature of 1650K and releases a large amount of energy (≈ 111.7kJ/mol of hydrazine). One issue is that at this temperature, the ammonia produced is unstable and itself decays via the reaction shown in **Figure 27**.

$$4/3\ NH_3 \longrightarrow 2/3N_2 + 4H_2 \text{ - Energy}$$

Figure 27: Thermal breakdown of ammonia.

This reaction is **slow and endothermic**, reducing the energy released in the decomposition reaction and subsequently reducing thrust. As this reaction is slow, the **dwell time** (the amount of time the fuel remains in the combustor), plays a large roll in the energy released. The full decomposition reaction for hydrazine can therefore be written as **Figure 28**.

$$3N_2H_4 \longrightarrow 4(1\text{-}x)NH_3 + (1\text{-}2x)N_2 + 6xH_2 + \text{Energy}$$

Figure 28: Full decomposition reaction for hydrazine.

Where $\boldsymbol{x}$ is the degree of ammonia dissociation. This parameter depends on the:

- Catalyst type
- Geometry
- Dwell time
- Size of chamber
- Chamber pressure

Note that the real schematic shown in the right of **Figure 25** has a very small combustor section, to ensure a low dwell time and thus increase thrust by reducing energy losses through the endothermic reaction of ammonia breakdown. Some key performance parameters for a hydrazine thruster are plotted in **Figure 29**.

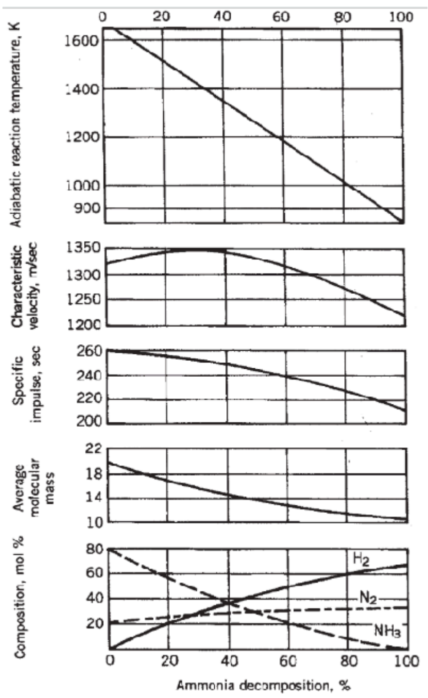

Figure 29: Performance parameters throughout a hydrazine decomposition reaction.

Note that the main parameter effecting the performance of the hydrazine thruster is the percentage of ammonia decomposition, meaning that dwell time is therefore one of the main contributing factors for engine performance.

6.3.2. Dangers of Hydrazine

Hydrazine is highly toxic, corrosive and flammable, meaning that working with this propellent is dangerous and costly. Some of the warning symbols related to hydrazine are shown in **Figure 30**.

Figure 30: Hazard symbols associated with hydrazine (1.flammable 2.corrosive 3.acutely toxic 4.serious health hazard 5.hazardous to the environment)

This provides motivation for the development of **green monopropellants** to decrease costs, allow for in-house refueling and ease of use.

6.3.3. Green Monopropellants: HAN

HAN or hydroxylammonium nitrate is an ionic liquid based compound which is solid at room temperature and often used in solid rocket motors. If mixed with water alcohol it becomes a monopropellant, the chemical formula as well as chemical structure are shown in **Figure 31**.

$[NH_3OH]^+ \, [NO_3]^-$

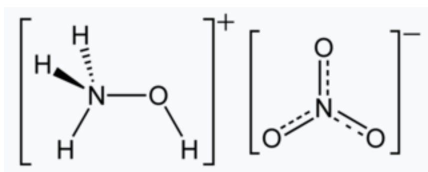

Figure 31: Chemical formula [Left] and chemical structure [right] of HAN.

6.3.4. Green Monopropellants: ADN

ADN or ammonium dinitramide is another ionic liquid based compound which is mixed with methanol, water and ammonia to yield a usable monopropellant. The chemical formula as well as the chemical structure are shown in **Figure 32**.

$[NH_4][N(NO_2)_2]$

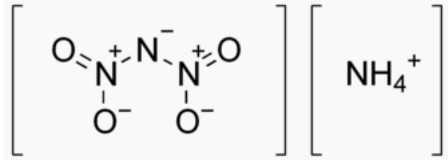

Figure 32: Chemical formula [Left] and chemical structure [right] of ADN.

6.3.5. Green Monopropellant: Hydrogen Peroxide

Hydrogen peroxide (H_2O_2) can also be used as a monopropellant where it decomposes over a catalyst bed into oxygen and water, however the efficiency of hydrogen peroxide as a monopropellant has a lower I_{sp} than the other monopropellant options.

6.3.6. Comparison of Green Monopropellants and Downsides

A table showing the performance of green monopropellents in comparison with traditional monopropellants (hydrazine) is shown in **Table 7**.

Name	Density g/m^3	Specific Impulse s	Temperature $°C$	Density Specific Impulse $s \cdot g/m^3$
Hydrazine	1.01	230	1120	232
ADN-based LMP-103S	1.24	244	1600	302
HAN-based AF-M315E	1.46	248	1900	362
98% Hydrogen Peroxide	1.439	198	955	285

Table 7: Performance of hydrazine vs green monopropellants

Some of the main downsides or caveats of green monopropellants are:

- **High temperatures** which require more exotic materials or active cooling.
- **Pre-heating of thruster** up to high temperatures to reach equilibrium temperature of reaction.
- Exact compositions are **owned by companies**.

6.4. Propellent Feed Mechanisms

There exist two main propellent feed mechanisms, these are **pressure driven** and **pump driven**. A system level image for both methods is shown in **Figure 33**.

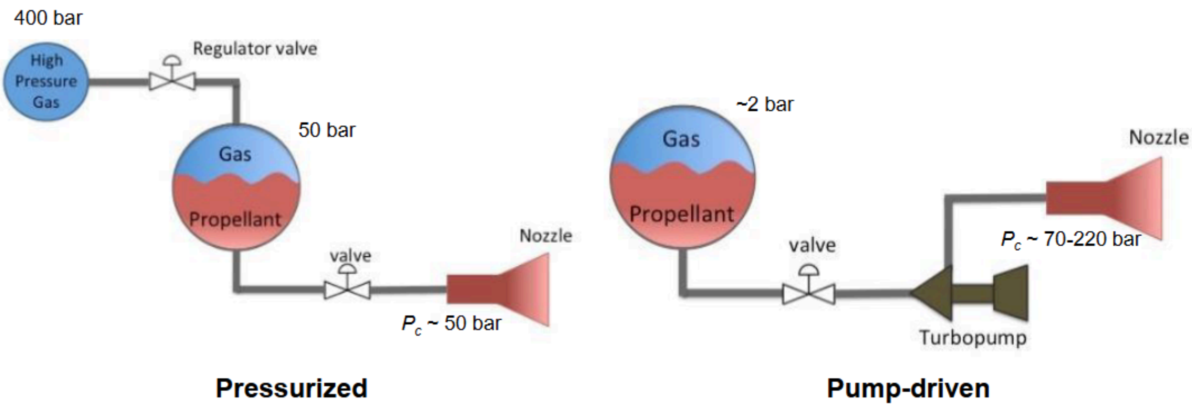

Figure 33: Pressure driven feed system [Left], pump driven feed system [Right]

For launch vehicles which require higher I_{sp}, higher thrust, higher pressures and higher flow rates a **pump driven** system is usually chosen. For spacecraft which require less weight, lower pressures and volume, a **pressure driven** system is chosen.

6.4.1. Pump Driven Propellent Systems: Turbopumps

Turbopumps pressurize the propellent before it enters the combustor, allowing for much higher pressures and flow rates. An example of a turbopump is shown in **Figure 34**.

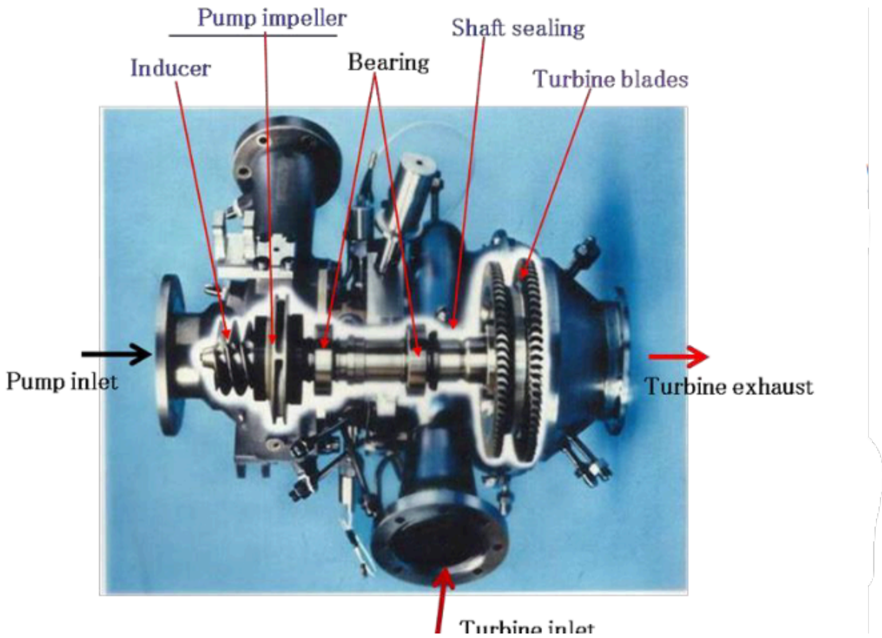

Figure 34: Spacecraft turbopump.

The working principle of a turbopump is that:

1. Propellent enters through the **propellent inlet**.
2. The **inducer** gradually increases the propellent pressure by a small bit, decreasing the chance of cavitation (like pre-stage fan in a jet engine).
3. **Impeller** increases the pressure and kinetic energy of the flow by rotating it axially out of the turbopump.
4. A **diffuser/volute** is placed at the exit of the impeller and converts any kinetic energy the flow has into static pressure.
5. This system is all driven by the **turbine** which is connected on the same shaft as the inducer and impeller. It takes hot energetic flow from the **combustor** and extracts work from it to drive the pump.

6.4.2. Pump Driven Propellent Systems: Open VS Closed Cycle

A pump driven propellent system can be categorized on whether the exhaust from the turbopumps is fed back into the main combustion chamber (**closed cycle**) or if it is dumped externally (**open cycle**). System level diagrams of these are shown in **Figure 35**.

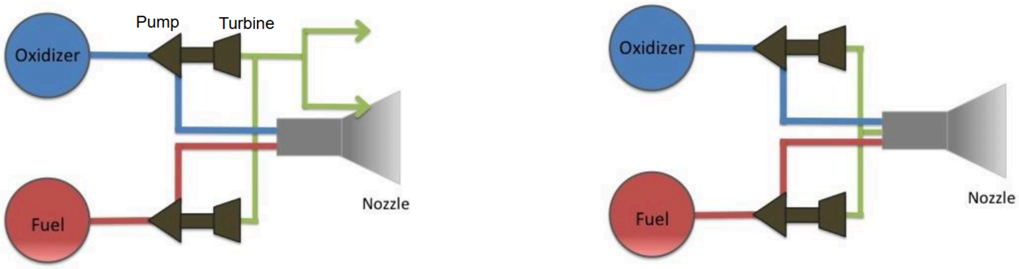

Figure 35: Open cycle propellent feed system [Left], closed cycle propellent feed system [Right].

While open cycle systems are simpler as the turbine's of the turbopump are operated at a lower relative pressure, the closed cycle systems offer higher efficiency (I_{sp}) at the cost of added complexity due to a much higher turbine pressure (turbine pressure must be close to or match combustion pressure.)

6.4.3. Open Cycle Pump Driven Propellent Systems: Gas Generator

In this system, a small amount of fuel and oxidizer are burnt in a **gas generator** (burnt **fuel rich**, keeping temperature low). The exhaust of the gas generator then powers the turbopumps. These systems are **simpler** and have a **lower mass** but have a **lower efficiency** (due to wasting fuel) than closed cycle systems by a few percent. An image of such a systems is shown in **Figure 36**.

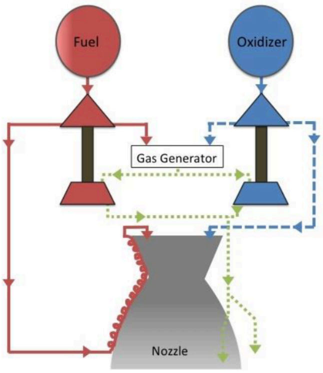

Figure 36: A system level image of a open cycle, gas generator, pump driven propulsion system.

6.4.4. Closed Cycle Pump Driven Propellent Systems: Staged Combustion

Similar to the gas generator system, some fuel and oxidizer are brunt in a **pre-combustor** which drives the turbines. The difference here, is that the exhaust is then piped into the main combustor. This system allows for **higher efficiencies** at the cost of **higher pre-combustor temperatures and pressures**. Note that the pre-combustor is less fuel rich than before, allowing for higher pressures. The pressure in teh pre-combustor **must be higher** than the main combustor to avoid backflow, increasing complexity. An image of such a systems is shown in **Figure 37**.

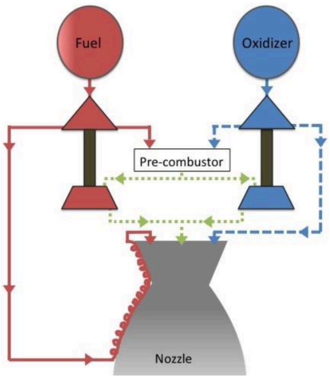

Figure 37: A system level image of a closed cycle, staged combustion, pump driven propulsion system.

6.4.5. Closed Cycle Pump Driven Propellent Systems: Expander Cycle

In this cycle, the turbines are driven by the fuel which is used to cool the nozzle. During the cooling process, the fuel is heated into a gas which is used to drive the turbines. Note that for this system, an initial starter or ignition is required in order to start the system. An image of such a systems is shown in **Figure 38**.

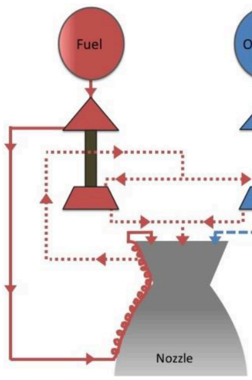

Figure 38: A system level image of a closed cycle, expander cycle, pump driven propulsion system.

6.4.6. Pump Driven Propellent Systems: Comparing cycles

	Merlin	RD-180	F-1	Raptor	BE-4	RS-25
Cycle	Open	Closed (LOX rich)	Open	Closed (Full Flow)	Closed (LOX rich)	Closed (Fuel Rich)
Fuel Type	RP-1	RP-1	RP-1	Methane	Methane	Hydrogen
Total Thrust	0.84 MN	3.83 MN	**6.77 MN**	2.00 MN	~2.40 MN	1.86 MN
Thrust : Weight	**198 : 1**	78 : 1	94 : 1	107 : 1	~80 : 1	73 : 1
Specific Impulse *(ISP)*	282 sl 311 vac	311 sl 338 vac	263 sl 304 vac	330 sl ~350 vac	~310 sl ~340 vac	**366 sl 452 vac**
Chamber Pressure	97 bar	257 bar	70 bar	**270 bar**	~135 bar	206 bar

Figure 39: Comparison of different pump driven rocket engines.

6.4.7. Pump Driven Propellent Systems: Alternative Cycles

One alternative cycle used in pump driven systems is **battery powered**. In this system, batteries drive the turbopumps instead of combustion of the propellent and oxidizer, saving on complexity. An example of this cycle is shown in **Figure 40**.

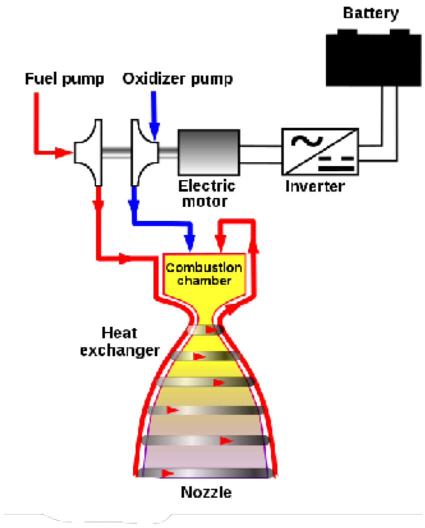

Figure 40: Battery powered propellent feed system schematic [Left], Rutherford engine which uses batter powered propellent feed system [Right].

7. Lecture 7

7.1. Pressurized Propellent Feed Systems

In pressurized propellent feed systems, a high pressure inert gas (such as helium) is fed into the tanks which pushes out the propellent. This means that the **propellent tanks need to have thick walls**, which means that the majority of the system mass is the propellent walls not the engine. Typically these systems are **used in space** and **yield lower thrusts, chamber pressures and performances**. A system level diagram of a pressure fed system is shown in **Figure 41**.

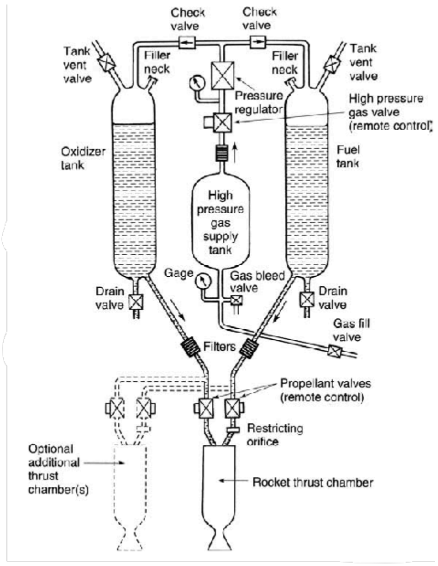

Figure 41: System level diagram of a pressure fed propellent system.

7.1.1. Pressurized Propellent Feed Systems: Blow Down

A **blow down** feed system is the most simple propellent feed system possible where the propellent tank is kept at a high pressure (30 - 40 Bar) which then decreases overtime as the propellent is used up (pressure is not topped up). These systems lead to a drop of pressure and therefore thrust over the lifetime of the engine. A system level image of this system as well as the pressure and thrust overtime are shown in **Figure 42**.

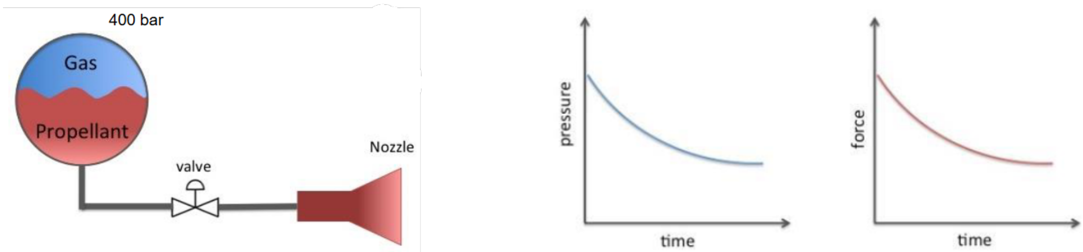

Figure 42: System level diagram of a blow down feed system [Left], thrust and pressure over time for a blow down system [Right].

7.1.2. Pressurized Propellent Feed Systems: Pressure Regulated

A **pressure regulated** system ensures that the pressure in the tanks remains the same overtime by topping up the tanks with an inert high pressure gas. These systems ensure optimal thrust over the lifetime of the engine at the cost of **complexity** as the **regulator valve** is complex and is needed to allow for the small opening of the valve to ensure constant pressure. A system level image of this system as well as the pressure and thrust overtime are shown in **Figure 43**.

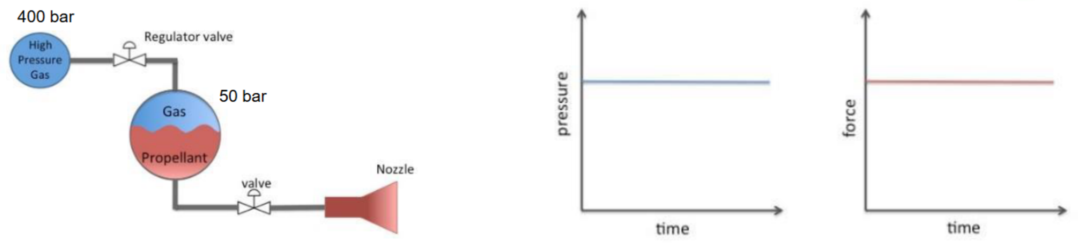

Figure 43: System level diagram of a pressure regulated feed system [Left], thrust and pressure over time for a pressure regulated system [Right].

7.1.3. Pressurized Propellent Feed Systems: Bang Bang

Bang bang systems are a variant of the **pressure regulated** system where instead of a regulator valve, a solenoid valve (bang bang valve) is used which can either be opened or closed. When the pressure in the propellent tank is below a certain value, the valve opens adding pressure until it reaches the cuttoff pressure when the valve closes. This allows for a **simpler system** at the cost of a **jagged thrust profile**. A system level image of this system as well as the pressure and thrust overtime are shown in **Figure 44**.

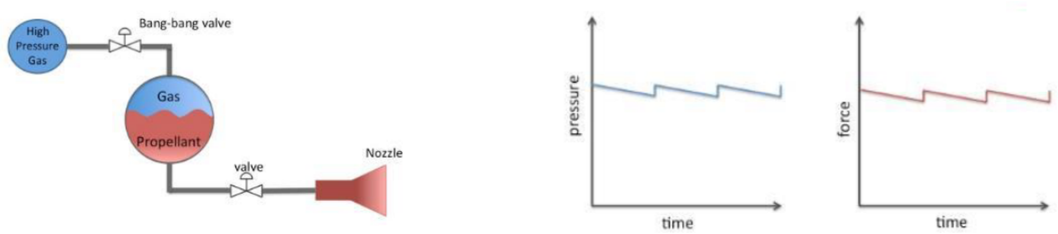

Figure 44: System level diagram of a bang bang feed system [Left], thrust and pressure over time for a bang bang system [Right].

7.2. Case Study: NASA Cassini Mission

The Cassini mission was a joint NASA ESA mission to investigate Saturn and its moon. The spacecraft was launched in 1997 by a Titan IV rocket and arrived at Saturn in 2004. The mission consisting of fly bys as well as the landing of a probe on Titan concluded in 2017. An image of the spacecraft is shown in **Figure 45**.

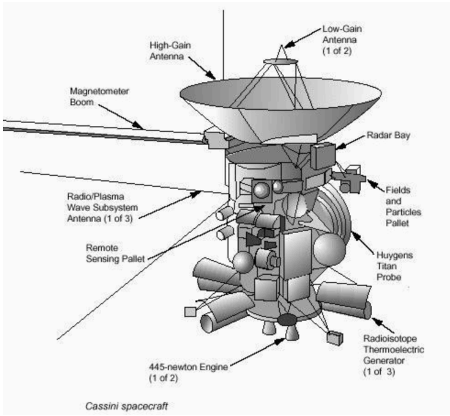

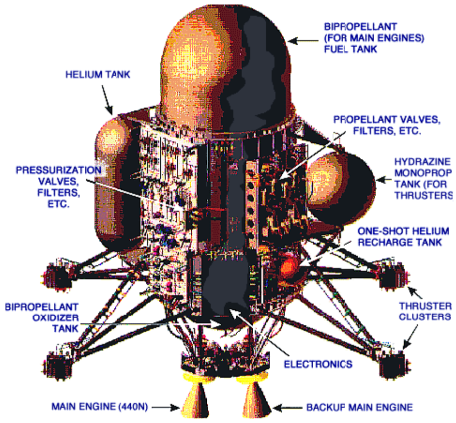

Figure 45: Labelled diagram of the Cassini probe [Left], labelled diagram of the propellent tanks and thrusters for Cassini [Right]

In terms of the propulsion system, the spacecraft used **MMH** for the fuel and **nitrogen textoroxide** for the oxidizer for the main engines whereas for the four attitude control thrusters, **hydrazine** was used. Both systems would have their pressure replenished by a high pressure helium tank. The propellent delivery schematic for the Cassini probe is shown in **Figure 46**.

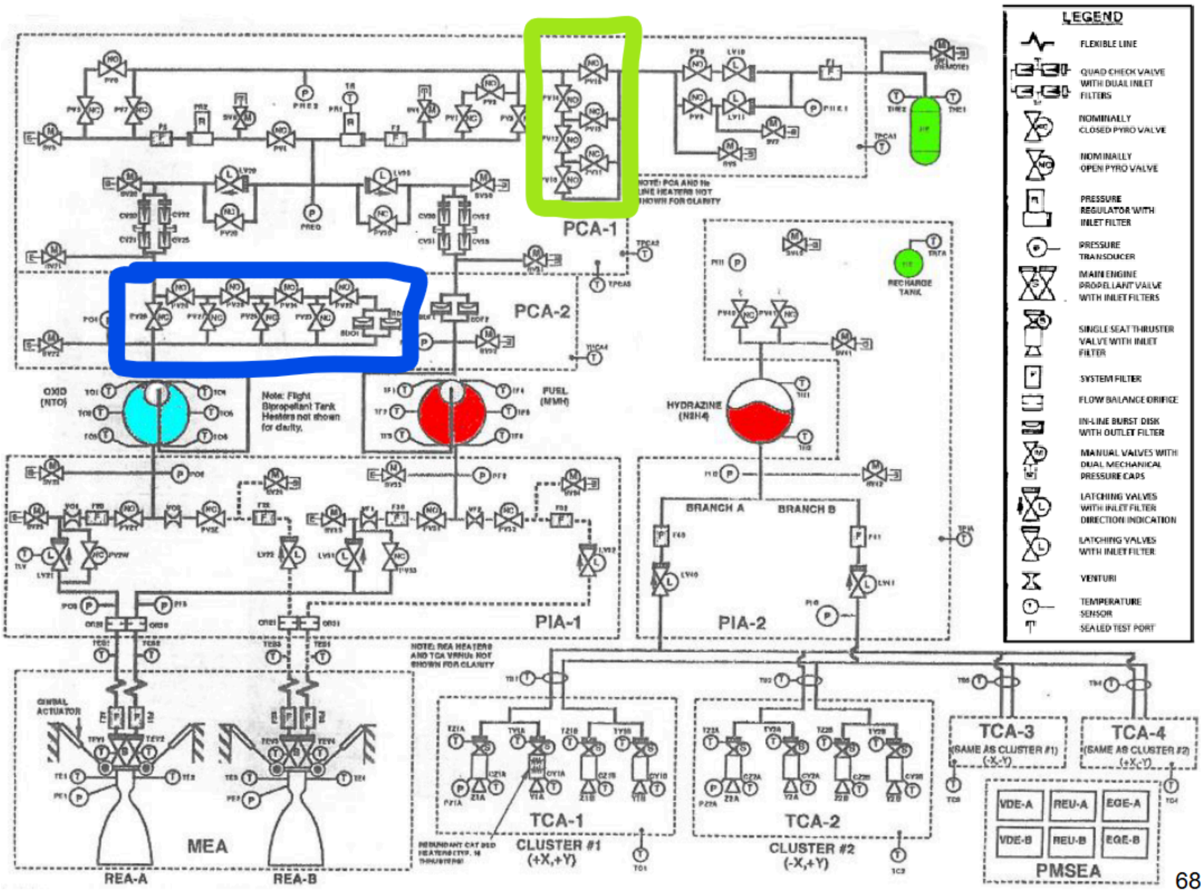

Figure 46: Cassini propellent dellivery schematic.

In th bottom right of **Figure 46**, the attitude control thrusters as well as the hydrazine tank are shown. On the left side of **Figure 46** shows the **pressure fed bipropellent** engine

($T \approx 400N$) with the MMH tank shown as light blue and the nitrogen textoroxide tank in red. The blue labelled section was a system of **pyro ladders** which controlled the pressure-regulated side of the system. The green was the redundant blow down system. Finally, every component had at least two levels of redundancy to the point that there were even two engines. A table detailing the different propulsion events for the mission is shown in **Figure 47**.

Event	Event or Phase End Date	Days From Launch	High ΔV (mps)	Pre-Maneuver Pressure (psia)	Pre-Maneuver Mass (kg)	Pyro Isolation Status
Launch	10/22/97	0	0	100	5609	Isolated
Press'n	11/13/97	22	0	250	5609	0-1-
TCM-1	11/16/97	25	24	250	5609	Regulated
Post Sat	12/15/97	55	0	250	5564	c-1
TCM-2	3/3/98	132	3.5	250	5564	Blowdown
TCM-3	4/12/98	172	0.3	243	5557	Blowdown
Venus-1	5/2/98	192	0	243	5557	-
TCM-4	5/22/98	212	25.6	205	5557	Blowdown
Repress	11/30/98	404	0	205	5509	0-2
DSM-1	12/2/98	406	435.4	25 L..	5509	Regulated
Isolate	12/3/98	407	0	250	4760	c-2
TCM-5	1/5/99	440	13.8	250	4760	Blowdown
TCM-6	4/25/99	550	0.6	245	4738	Blowdown
TCM-7	6/4/99	590	0.1	245	4737	Blowdown
Venus-2	6/24/99	610	0	245	4737	Blowdown
TCM-8	7/4/99	620	82.7	245	4737	Blowdown
TCM-9	7/19/99	635	6.8	218	4607	Blowdown
TCM-10	8/8/99	655	3.8	216	4597	Blowdown
Earth	8/18/99	665	0	215	45.91	-
TCM-11	9/7/99	685	45.7	204	4591	Blowdown
TCM-12	6/12/00	964	2.2	203	4521	Blowdown
TCM-13	10/10/00	1084	0.7	203	4518	Blowdown
TCM-14	12/9/00	1144	1	203	4517	Blowdown
Repress	6/1/04	2414	0	203	4515	0-3
SOI	7/1/04	2444	594	250	4515	Regulated,
PRM	9/16/04	2521	264	25 Q	3701	Regulated
Isolate	9/17/04	2522	0	250	3387	c-3
ODM	12/3/04	2599	38	250	3387	Blowdown
Tour	7/1/08	3905	497	246	3344	Blowdown
EOM	7/1/08	3905	0	203	2830	-

Figure 47: Cassini propulsive events.

Note that for important manuevers such as flybys the pressure regulated section of the system is used whereas for general manuevers the blow down section of the system is used.

7.3. Cold Gas Thrusters

These are the most basic thruster systems often used in **attitude control systems**, **micro or nano** satellites. These systems consis of a **high pressure gaseous propellent** is fed into a nozzle (flow controlled via valve) without any heating or reactions. Typically these systems are pressurized from **30 to 100 MPA** with **nitrogen being commonly used** due to its **inertness** as well as **low molecular mass** and relatively **high density**. The performance of different propellents is shown in **Table 8**.

Propellant	Molecular Mass (W)	Density (g/cm^3))	Ratio Specific Heats (k)	Theoretical (I_{sp})
Hydrogen	2.0	0.028	1.40	284
Helium	4.0	0.057	1.67	179
Methane	16.0	0.23	1.30	114
Nitrogen	28.0	0.39	1.40	76
Air	28.9	0.41	1.40	74

Propellant	**Molecular Mass (W)**	**Density (g/cm^3))**	**Ratio Specific Heats (k)**	**Theoretical (I_{sp})**
Argon	39.9	0.57	1.67	57
Krypton	83.8	1.19	1.63	50

Table 8: Theoretical performance of different cold gas propellent

However, the performances detailed in **Table 8** are only theoretical and in reality there are several losses in cold gas thrusters such as:

- Many molecules are very small meaning that the thrust produced by exhausting them is low.
- Over the nozzle, the temperature of the exhaust decreases which can go below the boiling temperature. This phase change sucks out energy, further decreasing performance.

In reality therefore, the thrust and performance of these engines is much lower, some real world cold gas thrusters are shown in

Thruster	**Max Thrust (N)**	**Chamber Pressure (MPA)**	**$I_{sp}(s)$**
Bradford Engineering PMT	0.002	0.25	60
Moog 58-118	3.6	1.59	65
RDMT-5	5		70
Vacco MIPS	55		65

Table 9: Real performance of different cold gas propellent

8. Lecture 8

START OF WEEK 4

8.1. Intro to Solid Propulsion

In there most primitive form, solid rocket boosters consist of a fuel and oxidizer that are bound together using a binder and are located within the combustion chamber itself. When ignited via an ignitor the mixture burns in place and is accelerated through a nozzle to produce thrust. Note that once ignited, solid rocket boosters cannot be stopped. They are used in two main scenarios, shown below. Note that the basic constituent parts of a SRB are shown in **Figure 48**.

- **Launch Vehicles**: The total required impulse is already known before launch and doesn't change so SRBs can be used.
- **When restarts are not needed**

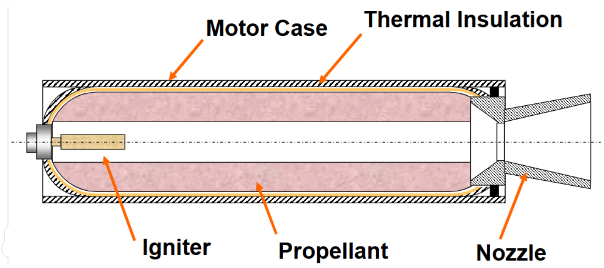

Figure 48: Constituent parts of a SRB.

8.2. Grain Shape and Thrust

Depending on the shape of the grain within the solid rocket motor, the thrust produced by the engine can vary. Various grain shapes and their associated thrust curves are shown in **Figure 49**.

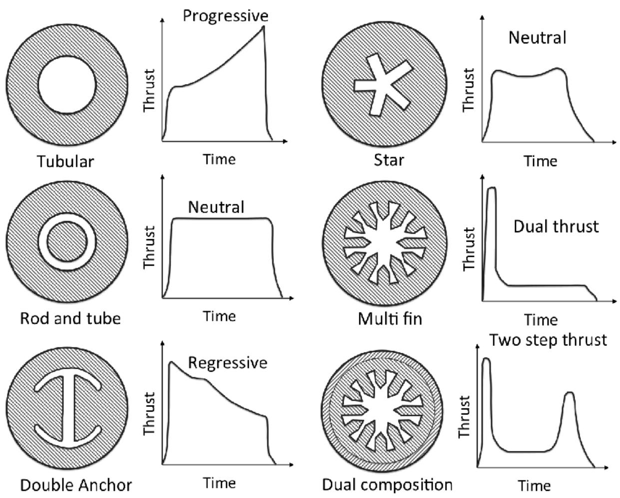

Figure 49: Effect of grain shape on the thrust profile..

The most common grain shape used is the **star** shape as this gives a quasi-constant thrust profile over the burn time. Note that for the **rod and tube** design, the tube can become easily dis-logged and cause issues. Typically SRBs will have a star grain pattern at the top with a tubular pattern below.

8.3. Mass Flow and Burning Rates

The equation for the mass flow rate of the exhaust of the solid propellent is given by **Eq. 42**

$$\dot{m} = A_b \dot{r} \rho_p \tag{42}$$

Where:

- $\dot{m}$: Mass flow rate (kg/s)
- $\dot{r}$: Burn rate (m/s)
- A_b: Burn area (m^2)
- ρ_p: Propellent density (kg/m^3)

The burn rate shown in **Eq. 42** is given by the empirical formula detailed in **Eq. 43**.

$$\dot{r} = aP_c^n \tag{43}$$

Where:

- P_c: Chamber pressure (Pa)
- a: Burn rate Coefficient,
- n: Burn rate exponent

The burn rate typically varies from 0.6 - 1.3 cm/s but can reach values of 5 cm/s in extreme cases. n typically varies from 0.2 - 0.6 with n > 1 leading to combustion instabilities.

8.3.1. Burning Effects: Burn Rate Exponent

The value of n controls how quickly the reaction flattens at a fixed burn rate, as shown in **Figure 50**.

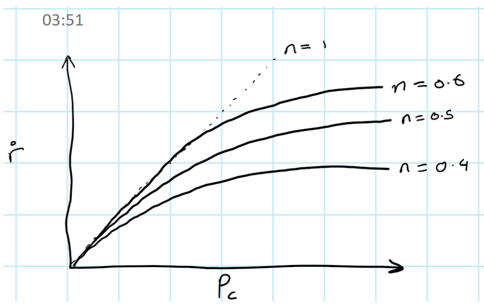

Figure 50: How changing n effects the burn rate.

Larger values of n mean an eventual higher burn rate and vice versa. Note that the value of $n = 1$ acts as a upper limit.

8.3.2. Burning Effects: Plateau and Mesa Burning

Plotting the burn rate on a log plot yields **Figure 51**. **Plateau** burning occurs when the binding material begins to breakdown and **Mesa** burning is another burning phenomena.

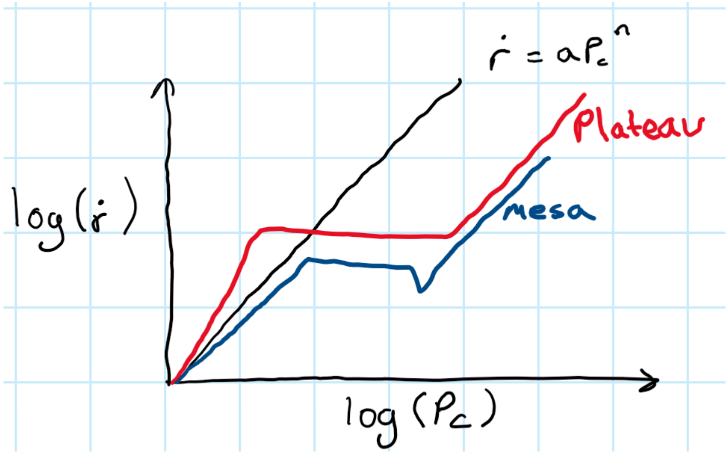

Figure 51: Mesa and Plateau burning.

8.3.3. Burning Effects: Ambient Temperature

Ambient temperature also has an effect on the performance as shown in **Figure 52**.

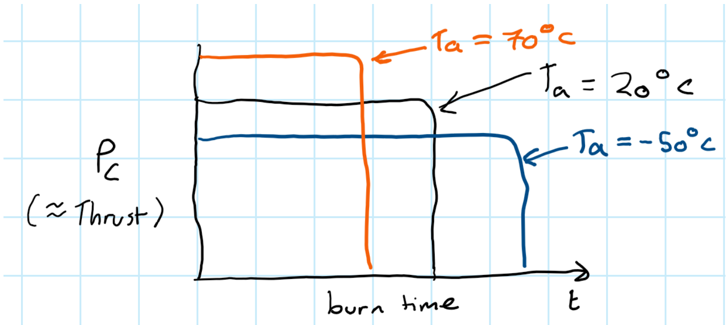

Figure 52: Effect of ambient temperature on thrust curve.

Note that higher ambient temperatures yield shorter burn times and vice versa. Note that the area under the graphs must remain constant as the amount of propellent doesn't change. The degree with which the temperature or pressure change with a given change in ambient temperature are given by the equations shown in **Eq. 44**.

$$\sigma_p = \left(\frac{\partial \ln(r)}{\partial T_b}\right)_{P_c} = \frac{1}{r}\left(\frac{\partial r}{\partial T_b}\right)_{P_c} \tag{44.1}$$

$$\pi_K = \left(\frac{\partial \ln(P_c)}{\partial T_b}\right)_K = \frac{1}{P_c}\left(\frac{\partial P_c}{\partial T_b}\right)_K \quad \text{Where } K = \frac{A_b}{A_t} \tag{44.2}$$

8.3.4. Burning Effects: Erosive Burning

Another parameter which effects the burning behavior is **erosive burning**, which occurs when high speed combustion products flow over the burning surface. An example where this can occur is if the inner radius of a tubular grain is similar to the throat area, this mean the edges of the grain near the throat see a non-zero velocity flow and so are burnt away quicker. An image depicting this example as well as the effect it has on the thrust curve is shown in **Figure 53**.

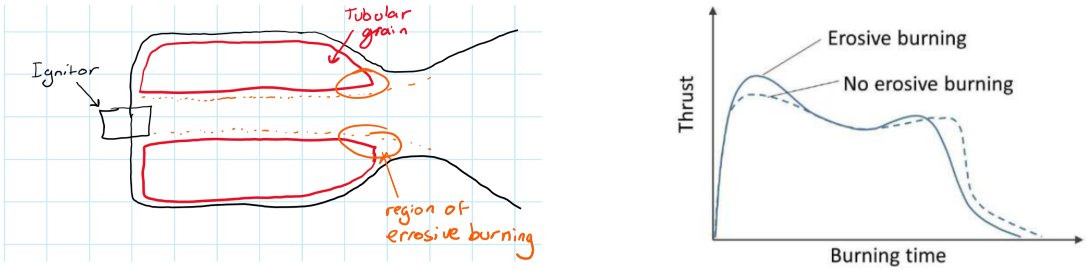

Figure 53: Diagram depicting erosive burning [Left], thrust graph overtime with and without erosive burning [Right].

8.3.5. Burning Effects: Acceleration

For an annular (or similar) grain where the burning occurs along the center of the rocket, spinning the rocket will **increase** the peak thrust whilst **reducing** the burn time, this is shown in **Figure 54**.

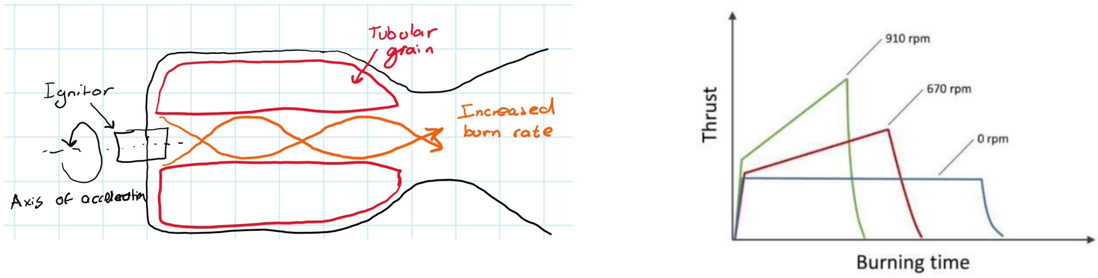

Figure 54: Diagram depicting burning under rotational velocity [Left], thrust graph overtime at various angular velocities. [Right].

In contrast, for a simple block of grain which is burning from the bottom, a lateral velocity will see a decrease in the peak thrust, this is shown in **Figure 55**.

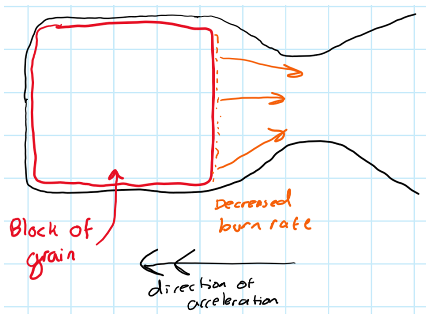

Figure 55: Diagram depicting the effect of lateral acceleration on a block grain.

8.3.6. Burning Effects: Metal Wires

The burning behavior can also be controlled through the embedding of metal wires, typically of silver or aluminum.

8.4. Solid Propellants

8.4.1. Double Base

A double base propellent consists of two monopropellent molecules where one is a **high energy** unstable molecule and the other is a **low energy** more stable gelling molecule. The most common double base propellent is nitroglycerin and nitrocellulose, shown in **Figure 56**.

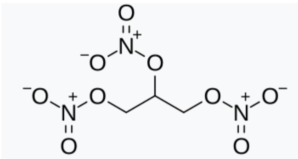

$C_3H_5N_3O_9$

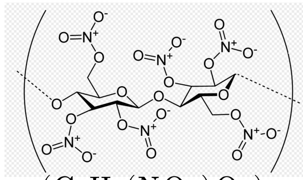

$(C_6H_9(NO_2)O_5)$

Figure 56: Molecular structure and chemical formula for nitroglycerin [Left], molecular structure and chemical formula for nitrocellulose [Right].

When nitroglycerin and nitrocellulose are burnt together, the nitroglycerin acts as the high-energy component and nitrocellulose acts as the stabilizer. When burnt together, these two monopropellents **burn smokeless**, have an $I_{sp} \approx 210$ and have a **low density**.

8.4.2. Composite

Composite propellents have a better performance than double base propellents and consist of multiple constituent parts which are:

- **Fuel**: Typically a metal powder (normally Aluminum).
- **Oxidizer**: Typically an inorganic salt (ammonium perchlorate).
- **Binder**: Forms the fuel and oxidizer into a rubber/cement like grain.

Some common fuels and oxidizers are shown in **Table 10**.

Name	Chemical Formula	Molecular Mass (W)	Density (kg/m^3)	Notes
Fuels				
Aluminium (powder)	Al	26.98	2.70	Widely used, good performance
Boron (powder)	B	10.81	2.34	High gravimetric and volumetric energy.
Magnesium (powder)	Mg	24.31	1.74	Easy ignition and high temp burning.
Oxidizers				
Ammonium Perchlorate	NH_4ClO_4	59.5	1950	High performance, low cost
Ammonium Nitrate	NH_4NO_3	60	1730	Smokeless, moderate performance, low cost
Sodium Nitrate	$NaNO_3$	56.4	2170	Moderate performance

Name	Chemical Formula	Molecular Mass (W)	Density (kg/m^3)	Notes
Potassium Perchlorate	$KClO_4$	46.2	2520	Moderate performance, low regression rate
Potassium nitrate	KNO_3	47.5	21120	Low cost, low performance
Binders				
Hydroxyl-Terminated Polybutadiene (HTPB)	$(C_4H_6)n(OH)_2$	54.09	0.90-0.92	Industry-standard inert binder but has a decent fuel contribution.
Glycidyl Azide Polymer (GAP)	$(C_3H_5N_3O)$ n	99.09	1.10-1.30	Energetic binder with higher performance than inert binders, more expensive, more sensitive.

Table 10: Common solid composite fuels, oxidizers and binders

8.5. Solid Propellant Performance

Plotting the performance of different solid propellent fuels against their burn rates yields **Figure 57**. Note that the maximum I_{sp} of a solid rocket motor is only 250s which is less much less than a chemical rocket. Also the method of by which the solid grain is form (extrusion or casting) further effects the performance. Finally their are hybrid grains which are both double base and composite as is shown in the figure.

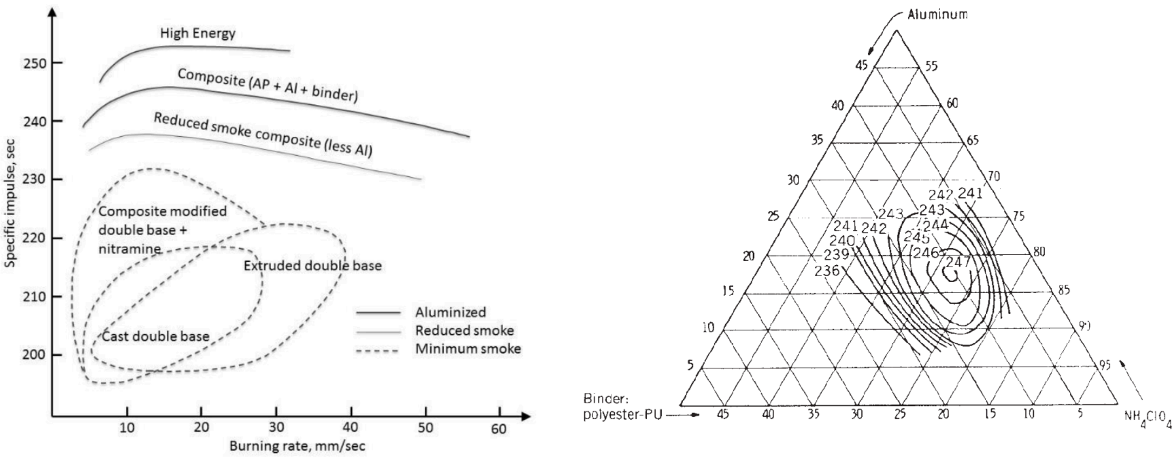

Figure 57: Performance against burn rate for different solid rocket propellents [Left], solid composite fuel performance [Right].

On the right of **Figure 57**, there is a graph which shows the performance of different percentage makeups of the oxidizer, fuel and binder for a composite fuel.

8.6. Real Solid Propellant Makeup

The realistic makeup of a double base, composite and hybrid double base composite solid fuel are shown in **Table 11**.

Double Base		Composite		Composite Modified Double Base	
Ingredient	**Mass %**	**Ingredient**	**Mass %**	**Ingredient**	**Mass %**
Nitrocellulose	51.4	Ammonium perchlorate	70.0	Ammonium perchlorate	20.4
Nitroglycerine	43.0	Aluminium powder	16.0	Aluminium powder	21.1
Diethyl phthalate	3.2	Polybutadiene acrylonitrile copolymer	11.78	Nitrocellulose	21.9
Ethyl centralite	1.0	Epoxy curative	2.22	Nitroglycerine	29.0
Potassium sulfate	1.2			Triacetin	5.1
Carbon black	< 1			Stabilizers	2.5
Candelilla wax	< 1				

Table 11: Makeup of different solid rocket fuels.

Note that **Diethyl phthalate** is a plasticizer which is added to the double base to allow for easier moulding. **Carbon black** is added in small quantities as an opacifier to make the grain darker and thus reduce radiative heating. **Candelilla wax** is added to make it easier for the grain to escape the mould.

8.7. Solid Propellent Flame Structure

Double base solid rocket fuels feature the fuel and oxidizer bound together on the same molecule allowing for a smokeless clean burn. However for composite fuels, the oxidizer is separate from the fuel leading to a much more chaotic and uncontrolled burn, these effects are depicted in **Figure 58**.

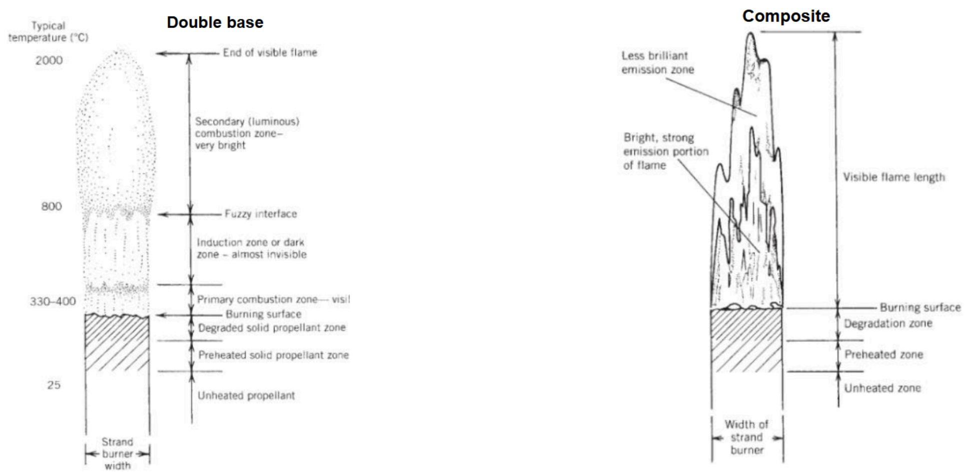

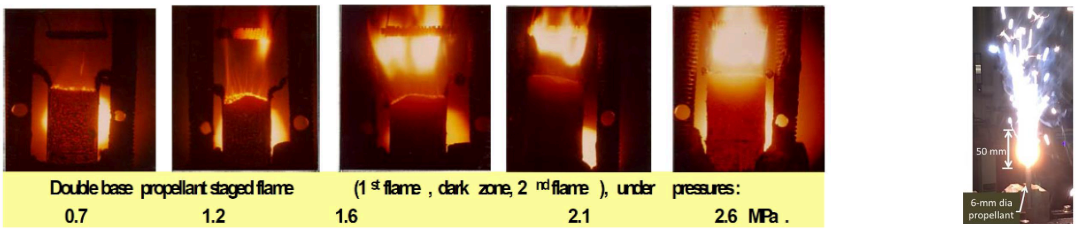

Figure 58: Double base fuel flame structure [Top Left], Composite fuel flame structure [Top Right], Real double base flame [Bottom Left], Real composite flame structure [Bottom Right]

8.8. Solid Rocket Ignition Systems

For different scales of solid rocket motor there exists two different types of ignition systems, these are explained below and shown visually in **Figure 59>**.

- **Pyrotechnic Ignitor**: Generate a hot flame via explosives or energetic propellant-like formulations.
- **Pyrogenic Ignitor**: Essentially a small solid rocket motor optimized for heat not thrust.

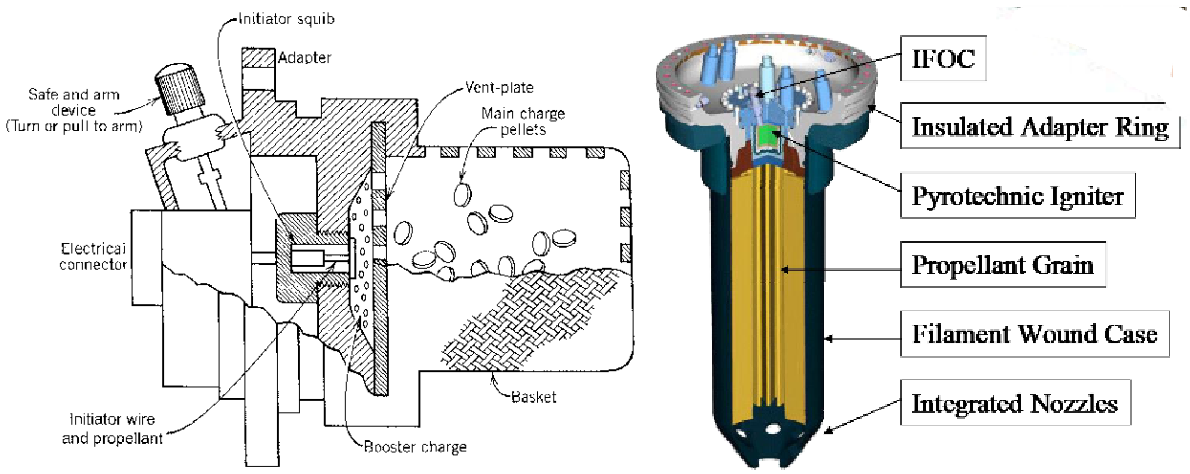

Figure 59: Pyrotechnic ignitor [Left], pyrogenic ignitor [Right]

For pyrotechnic ignitors, an initial arc may combust a squib, which then combusts a booster or intermittent charge (made from a excitable solid fuel formulation) which then ignites a basket of fuel (disks of solid rocket fuel) which is then vented into a solid rocket motor. for pyrogenic ignitors, a pyrotechnic ignitor first ignites a small solid rocket motor optimized for heat which is exhausted into the main solid rocket motor.

8.9. Hybrid rockets

A hybrid rocket is a combination of a bipropellent liquid and solid rocket. A typical hybrid rocket consists of a liquid oxidizer with a solid fuel. The inverse configuration does exist but is rarely used. An image depicting the key components of a solid rocket motor are shown in **Figure 60**.

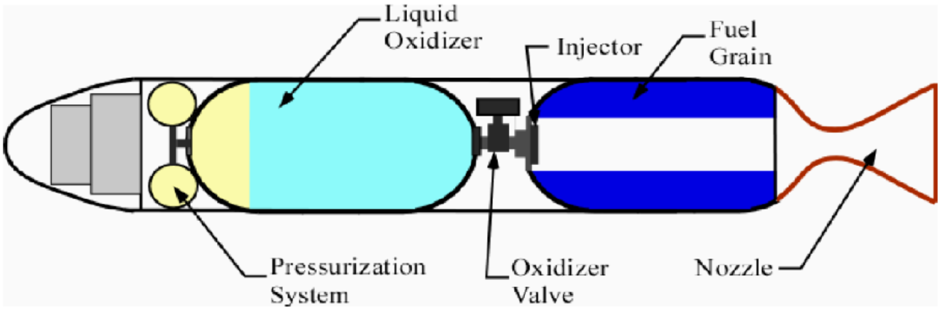

Figure 60: System level diagram of a hybrid solid rocket motor.

8.9.1. Advantages of Hybrid Rockets

Some key advantages of hybrid rockets over liquid bipropellent rockets and solid rockets are listed below. The performance of all three rocket motor types is shown in **Table 12**.

- Safer and relatively simpler than liquid bi-propellant and solid rockets.
- Has start, stop and throttling capabilities which are not present on solid rockets.
- Have a higher I_{sp} than solid rocket motors.

Type	I_{sp} at Sea Level	Thrust Range (N)
Solid	$<$ 250s	$\leq 10^7$
Liquid bipropellent	H_2/LOX: 380s	$\leq 10^7$
	RP1/LOX: 300s	
Hybrid	300s	$\leq 10^6$

Table 12: Comparative performance of liquid bipropellent, solid and hybrid rockets.

8.9.2. Disadvantages of Hybrid Rockets

Some key disadvantages of hybrid rockets over liquid bipropellent rockets and solid rockets are listed below. Note that the biggest problem with hybrid rockets are the low fuel regression rates.

- No independent control of fuel mass flow rate which effects combustion.
- O/F mixture ratio (and performance) may vary due to variable **fuel regression rate** (typically $<$ 1mm/sec, which limits thrust).
- Poorly known or understood due to small number of examples.
- Typically lower performance than for liquid bipropellant.
- Prone to large-amplitude, low-frequency pressure fluctuations (chugging) and higher frequency flame instabilities.

9. Lecture 9

9.1. Hybrid Rocket Combustion

Combustion within a solid rocket motor is much more complex than the combustion that takes place in solid or liquid rockets, as shown in **Figure 61**.

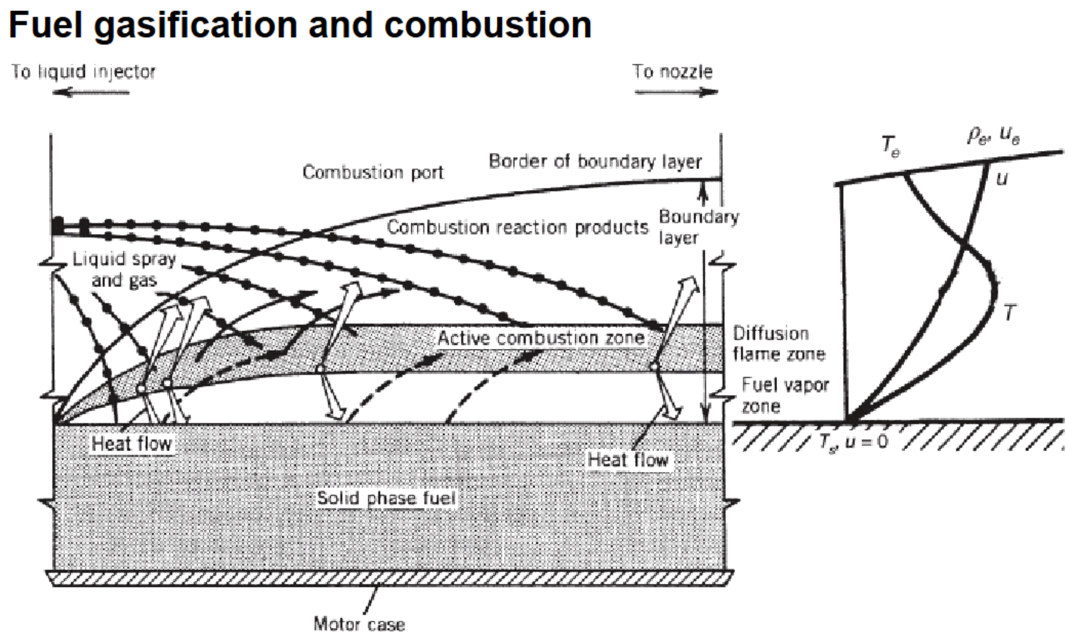

Figure 61: Combustion for hybrid rockets.

Note that there is a **highly turbulent boundary layer** which forms on the surface of the fuel grain. Heat is transferred through convection and radiation through the boundary layer into the fuel grain which evaporates it and allows for combustion to take place, due to this complex mechanism, the regression rates for the fuel grain are **typically one third of that of solid rockets**. The fuel surface regression rate against the flow rate of oxidizer is shown in **Figure 62**.

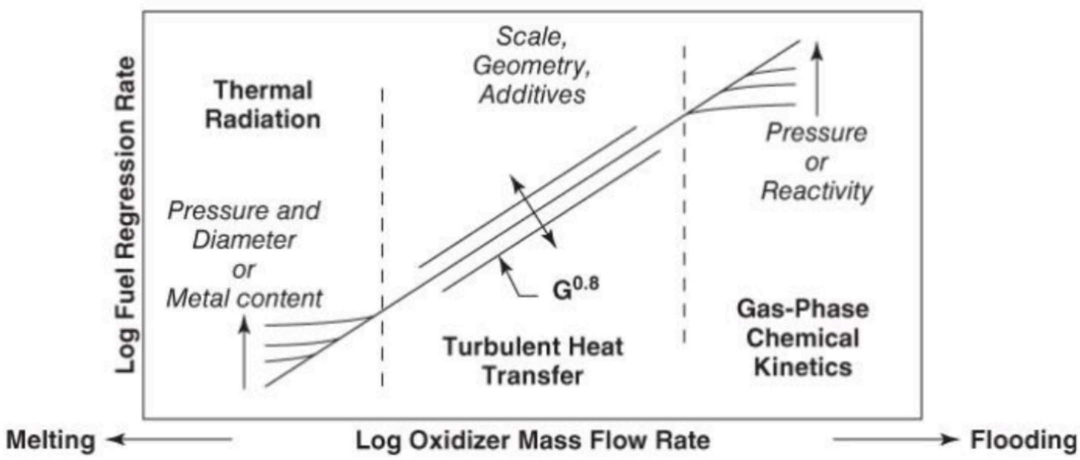

Figure 62: Plot of oxidizer flow rate against fuel regression rate.

For **low oxidizer flow rates** the heat transfer is **radiation dominated** and the fuel regression rate is low. For **intermediate values of oxidizer flow rate**, the heat transfer is **convection dominated** with the turbulent boundary layer behavior seen in **Figure 61**. Finally at very **high oxidizer flow rates** phase change and chemical kinetics take over.

9.2. Hybrid Rocket Equations

Using **Figure 62**, equations for teh regression rate as well as the mass flow rate can be generated, teh equation for regression rate is shown in **Eq. 45**.

$$\dot{r} = aG_{ox}^n = a\left(\frac{\dot{m}_{ox}}{N\pi R_p^2}\right)^n \tag{45}$$

Where:

- $\boldsymbol{G_{ox}}$: Oxidizer mass flux (kg/m^2s)
- $\boldsymbol{\dot{m}_{ox}}$: Oxidizer mass flow rate (kg/s)
- $\boldsymbol{N}$: Number of circular ports
- $\boldsymbol{R_p}$: Radius of circular ports (m)

Note that in **Eq. 45**, the empirical exponent n typically ranges between 0.4 - 0.8. **Eq. 45** can then be substituted into the equation for mass flow rate, **Eq. 42**, to yield **Eq. 46**.

$$\dot{m}_f = \rho_f A_p(t)\dot{r} = 2\pi^{1-n}\rho_f N^{1-n} a\dot{m}_{ox}^n R_p^{1-2n} L \tag{46}$$

Where:

- $\boldsymbol{\rho_f}$: Fuel grain density (kg/m^3)
- $\boldsymbol{A_p}$: Fuel grain surface area (m^2)
- $\boldsymbol{L}$: Fuel grain length (m)

Note that the value of the empirical exponent n in **Eq. 46** effects the behavior of R_p in the following ways:

- for n $<$ 0.5 fuel mass flow rate increases as Rp increases
- for n $>$ 0.5 fuel mass flow rate decreases as Rp increases
- for n = 0.5 fuel mass flow rate remains constant as Rp increases

9.3. Hybrid Rocket Propellents

Typical hybrid rocket oxidizers are:

- Nitrous oxide, hydrogen peroxide, LOX, Hydroxyl ammonium nitrate

Typical hybrid rocket fuel grains are (parrafin wax used to increase regression rate):

- HTPB, PBAN, rubber, paraffin wax

Note that hybrid rockets are an area of on going research with exotic propellent and various embeddings being looked into.

9.4. Injectors

START OF WEEK 5

An injector sits at the top of a combustion/decomposition chamber and has a few main purposes, these are:

- Introduce the liquid (fuel or oxidizer or both) into the combustion chamber and meter its flow rate.
- Cause the liquid to break up into smaller drops.
- Distribute and mix the propellants.
- Isolate the propellant tank from the thruster chamber through a suitable pressure drop across the injector.

Note that the pressure drop is very important, or combustion instabilities will cause up stream issues and effect flow rates. There are three main types of injectors that are used, and these are detailed in the following sections.

9.4.1. Orifice Injector

Also known as a hole injector, this class of injectors consist of holes through which the liquid is fed through. Typically these are designed with alternating holes of fuel and oxidizer and the spray from the holes is designed to impinge on adjacent holes. An image of a orifice injector is shown in **Figure 63**.

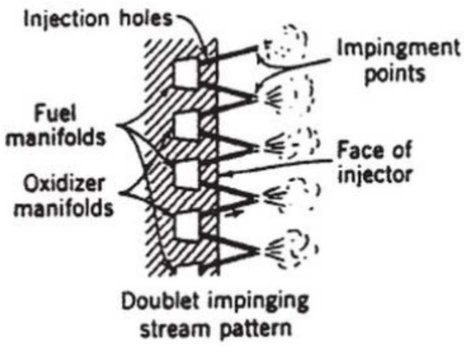

Figure 63: Image of an orifice injector.

9.4.2. Spray Injectors

This class of injectors inject the liquid into a cylindrical chamber where it swirls around and is then released into a conical jet shape **Figure 64**.

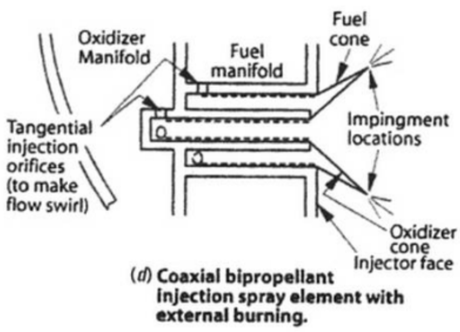

Figure 64: Image of a spray injector.

9.4.3. Pintle injectors

This class of injectors sprays one liquid into an internal channel with a 90 degree turn at the end. The other liquid is then sprayed on the outside of the channel, meaning when both liquids meet they mix and form a conical plume. This injector is shown in **Figure 65**.

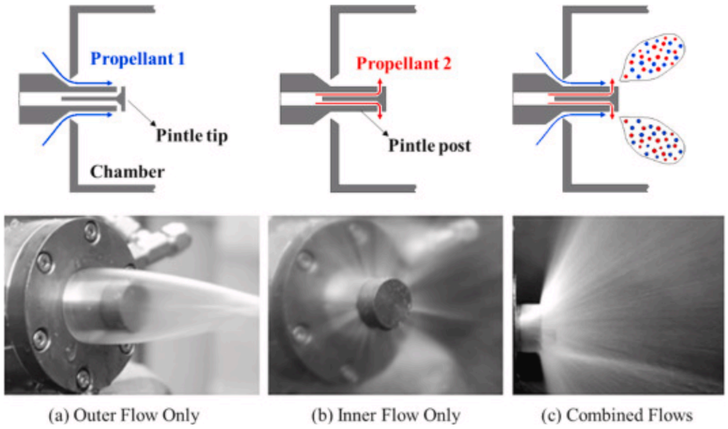

Figure 65: Image of a pintle injector.

9.4.4. Orifice Pressure Drop

The equation for the pressure drop across an orifice type injector can be calculated by considering the change inn pressure being equal to the dynamic pressure and using the mass flow rate equation. This expression is shown in **Eq. 47**.

$$\dot{m} = C_d A \sqrt{2\rho \Delta P} \quad \longrightarrow \quad \Delta P = \frac{1}{2\rho}\left(\frac{\dot{m}}{C_d A}\right)^2 \tag{47}$$

Where C_d is the coefficient of discharge and is present as $A_{\text{eff}} < A$. A typical range for the pressure drop is 0.2 - 0.3 P_c, any higher and **energy is being wasted**, any lower and **combustion oscillations will effect the upstream flow**. Typical values for $C_d \approx 0.65 - 0.7$. To determine C_d empirically, $\dot{m}$ would be plotted against $\sqrt{\Delta P}$ for water flowing through the nozzle. This gives the gradient of the straight line (through the origin) as $C_d A\sqrt{2\rho}$, which allows for the calculation for C_d.

10. Lecture 10

10.1. Thrust Chambers

The thrust chamber is where combustion/burning occurs. Here liquid propellent is injected, atomized, vaporized, mixed and burnt. Chamber volume is typically maximized and depends on heat, propellent used, heating and manufacturing constraints. The key dimensions for a thrust chamber are shown in **Figure 66**.

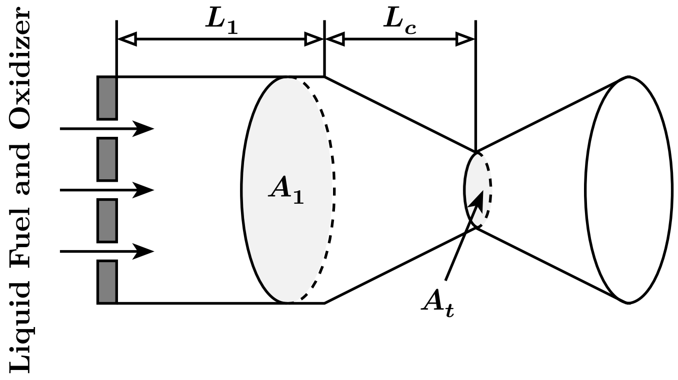

Figure 66: Thrust chamber dimensions.

Note that in **Figure 66**, the dimensions of the thrust chamber are simplified into conical sections. The volume of a combustion chamber is a key parameter and its formula is shown in **Eq. 48**.

$$V_c = A_1 L_1 + \frac{1}{3} A_1 L_c \left(1 + \sqrt{\frac{A_t}{A_1}} + \frac{A_t}{A_1}\right) \qquad L* = \frac{V_c}{A_t} \tag{48}$$

Where:

- $\boldsymbol{V_c}$: Combustion volume (m^3).
- $\boldsymbol{L_1}$: Cylindrical section length (m).
- $\boldsymbol{A_t}$: Throat area (m^2).
- $\boldsymbol{A_1}$: Cylindrical section area (m^2).
- $\boldsymbol{L_c}$: Converging section length (m).
- $\boldsymbol{L*}$: Characteristic length (m).

For the characteristic length shown in **Eq. 48**, $L* \approx 0.8 - 3m$ and for monopropellants this value is even higher. The stay time for a droplet of fuel within the combustion chamber is shown in **Eq. 49**.

$$t_s = \frac{V_c}{\dot{m} V_1} \tag{49}$$

Where t_s is the stay time and V_1 is the the volume per unit mass of propellant within the chamber. The stay time defines the time for vaporization, mixing and combustion of the propellant and is experimentally determined with $t_s \approx 0.001 - 0.04s$.

10.2. Thrust Chamber: Heat Transfer

Thrust chambers can reach very high temperatures due to the combustion and compression that takes place within them (for monopropellant $1000K$ and for bipropellant $3000K$). Nozzles must be designed to withstand this temperature as well as the associated stresses and the pressure from the exhaust itself. The temperature variation across a nozzle is shown in **Figure 67**.

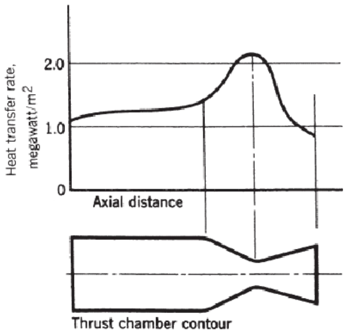

Figure 67: Temperature variation over a nozzle.

These high temperatures require some form of cooling in order to stop the nozzle and combustion chamber from melting.

10.2.1. Radiation Cooling

In this method of cooling, a material is chosen with a high emissivity is chosen which allows for heat to be radiated away from the nozzle. This method works well for small - medium engines as well as engines beyond a certain expansion ratio. The material used must be able to withstand high temperatures, some commonly used materials are Niobium, rhenium, and carbon-carbon composites.

10.2.2. Regenerative Cooling

This method of cooling is widely used in launch vehicles and large engines. In this method a liquid (typically the fuel) flows around the nozzle and thrust chamber before it is fed into the combustion chamber, cooling the nozzle and thrust chamber. In this method **no energy is lost** and specific cooling can be achieved by varying the diameter and number of cooling channels. An image of a regenerativly cooled nozzle is shown in **Figure 68** and the associated temperature variation across the wall is shown in **Figure 69**.

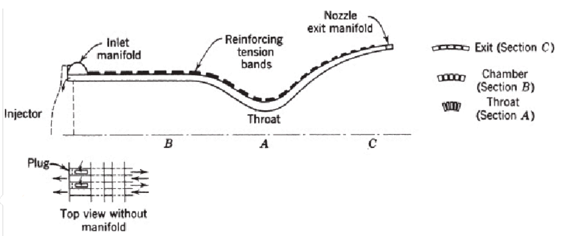

Figure 68: Cross sectional schematic of a nozzle with regenerative cooling.

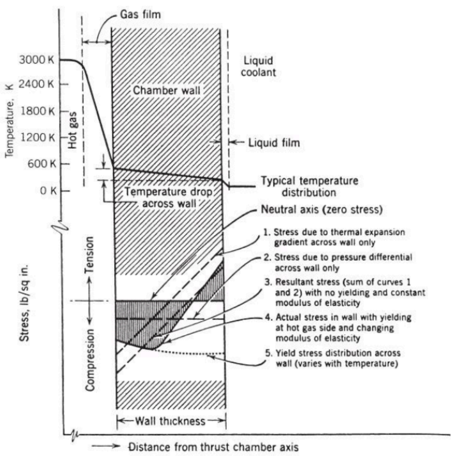

Figure 69: Temperature and stress variation across the nozzle wall of a regenerativly cooled engine.

Note that in **Figure 69**, the stress variation across the wall is dominated by the thermal expansion gradient and not the hoop stress, causing a high stress reversal and complex stress state.

10.2.3. Film Cooling

This method of cooling is where a small amount of liquid (typically fuel) is injected (using injectors at the wall or top of teh chamber) along the wall to reduce the heat transfer. If fuel is injected, the oxygen/fuel ratio is altered, reducing the amount of combustion that takes place keeping the wall cool. However, film cooling **is only used as a secondary method** and it can also **cause significant performance reductions** due to the change on oxygen/fuel ratio. An image of film cooling is shown in **Figure 70**.

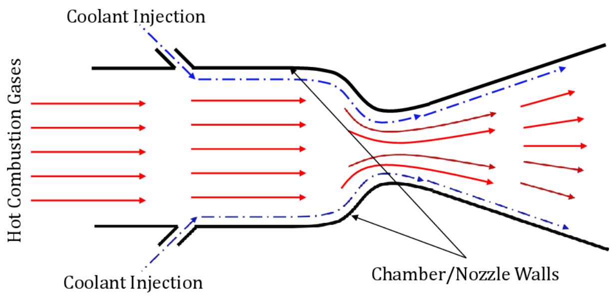

Figure 70: Film cooling employed

10.2.4. Ablative cooling

This method of cooling uses an layer of organic compound which at a certain temperature combusts and breaks away, removing heat energy with it. Typically, the liner consists of a fibre and resin (phenolics are used often) and can only be used as long as the ablative material exists within the engine. Ablative cooling is typically used **in solid rocket motors** where film and regenerative cooling cannot take place, an image of an ablatively cooled combustion chamber and nozzle are shown in

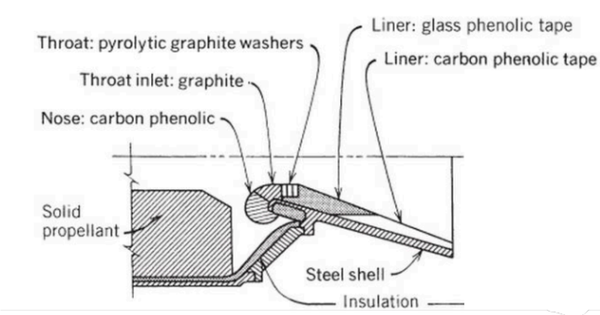

Figure 71: Ablative cooling on a solid rocket motor's nozzle and thrust chamber

10.3. Monopropellant Bed Loading

For monopropellent systems, it is important that the amount of catalyst is optimized, too much and there is wasted mass, type little and the bed is flooded, stopping decomposition from taking place. For a given thruster, a bed loading parameter, G is known and using this parameter the area of the catalyst bed can be calculated using **Eq. 50**.

$$G = \frac{\dot{m}}{A_1} \tag{50}$$

Where:

- $\boldsymbol{G}$: Catalyst bed loading (kg/sm^2)
- $\boldsymbol{A_1}$: Catalyst bed area (m^2)
- $\boldsymbol{\dot{m}}$: Propellent flow rate (kg/s)

Typically for small thrusters $G \approx 1 - 10kg/sm^2$ and for large rockets $G \approx 10 - 100kg/sm^2$. Once the value of G is known for a thruster, the catalyst bed can be sized using this equation.

11. Lecture 11

START OF WEEK 6

11.1. Introduction to Electric Propulsion

Electric propulsion is the process of **accelerating propellent using electricity.** Typically electric proplusio systems feature **much higher exhuast velcoities** than comparible chemcical and solid thrusters (and therefore **much higher I_{sp}s**) at the cost of **lower thrust** ($F_{max} \approx 5N$). As shown in **Figure 1**, there are three main groups of electric propulsion systems, electrothermal, electrostatic and electromagnetic.

11.1.1. Overview of Electrothermal Propulsion Systems

Electrothermal systems use electricity to heat up a gas which is then passed through a nozzle. The two main systems used to heat up the gas are resistors in **Resistojets** and electrical arcs in **Arcjets**.

11.1.1.1. Overview of Resistojets

Resistojets are a subset within electrothermal propulsion systems which use an electrical current running through knife-edge-like wires which heat upm liquid propellent passing over them. Internal baffles and insulation are used to keep the temperature within the chamber high. A schematic drawing of a resistojet thruster is shown in **Figure 72**.

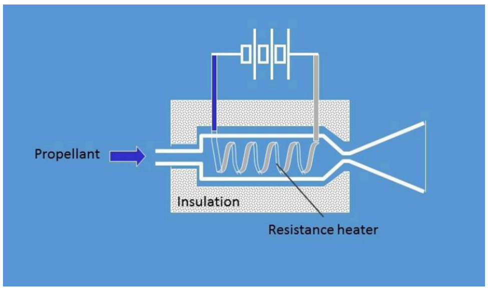

Figure 72: Schematic diagram of a Resistojet.

11.1.1.2. Overview of Arcjets

Arcjets are a subset within electrothermal propulsion systems which use a high potential difference between an anode and cathode to create a spark which then heats up a propellent. Although the spark is difficult to create and maintain, these systems can heat the propellent up to much higher temperatures than resistojet systems as the heating is no longer material limited. A schematic drawing of an arcjet thruster is shown in **Figure 73**.

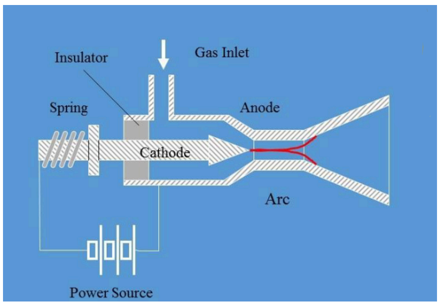

Figure 73: Schematic diagram of a Arcjet.

11.1.2. Overview of Electrostatic Propulsion Systems

Electrostatic propulsion systems make use of Coulombs force to accelerate and focus ions to generate thrust. The exhaust is then neutralized by introducing electrons into it. The two main electrostatic thrusters used are **grided ion thrusters** and **electrospray/FEEP thrusters**.

11.1.2.1. Overview of Gridded Ion Thrusters

In this system, propellent is fed into a chamber where it is ionized (using either an electron gun, RF energy or a microwave system). The resulting plasma then sits at thousands of volts, eventually an ion will move towards the grid where it is rapidly accelerated due to the high negative charge creating thrust. An schematic image of a gridded ion thruster is shown in **Figure 74**.

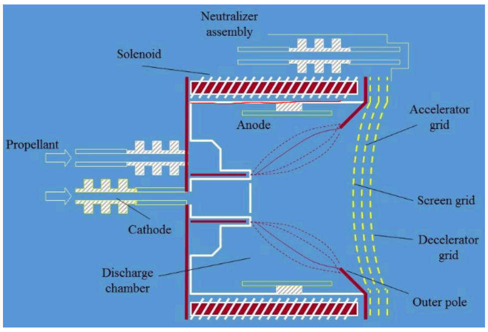

Figure 74: Schematic diagram of a gridded ion thruster.

11.1.3. Overview of Electrospray Thrusters

In this system, liquid is fed into a needle where it coalesces into a fluidic cone. A large voltage is then applied to the end of the needle and charged ions or ions are accelerated out into a spray. Although this system is simple, it is difficult to achieve and control. Organic liquids or metals can be used, an schematic diagram of an electrospray thruster is shown in

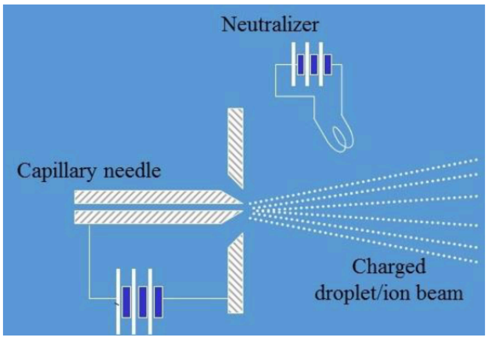

Figure 75: Schematic diagram of a electrospray thruster.

11.1.4. Overview of Electromagnetic Propulsion Systems

Electromagnetic propulsion systems use electricity to ionize a flow of propellent and then accelerate the resulting positive ions using a strong electric and magnetic field (utilizing the right hand rule to generate a force). The two main types of electromagnetic thrusters are **pulsed plasma thrusters** and **magneto plasma dynamic (MPD) thrusters**.

11.1.4.1. Overview of Pulsed Plasma Thrusters

Pulsed plasma thrusters are a simple form of electromagnetic thruster which creates an arc between a highly positively and negatively charged plate which then ablates away a small amount of a Teflon block. This is then accelerated out of teh thruster using the Lorenz force. A schematic diagram of this thruster is shown in **Figure 76**.

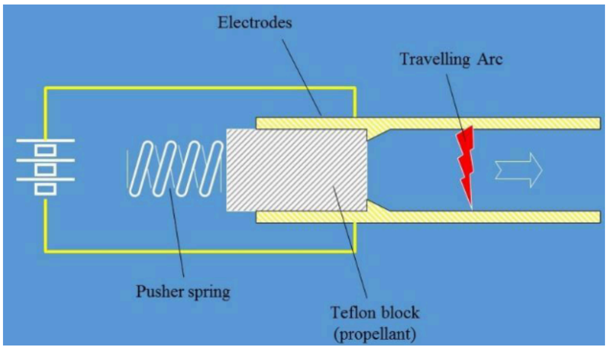

Figure 76: Schematic diagram of a pulsed plasma thruster.

11.1.4.2. Overview of Magneto Plasma Thrusters (MPDs)

MPDs are similar in design to arcjets however they operate at much higher currents. Whereas arcjets may operate at 10s of amps, MPDs may operate at 100k amps. This allows for much more ionization of the propellent into a plasma which can be further accelerated using the Lorenz force. A schematic diagram of a MPD is shown in **Figure 77**.

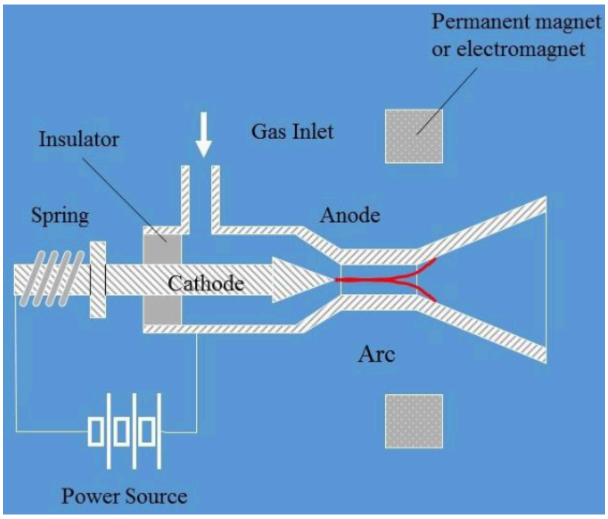

Figure 77: Schematic diagram of an MPD thruster.

11.2. Overview of Hall Effect Thrusters

These thrusters sit between electromagnetic and electrostatic thrusters, and are the dominant form of space propulsion. Whilst propellent does get ionized in a chamber and accelerated towards a negative grid, Hall effect thrusters also feature an annular chamber with a magnetic field also present. A schematic image of a Hall effect thruster is shown in **Figure 78**.

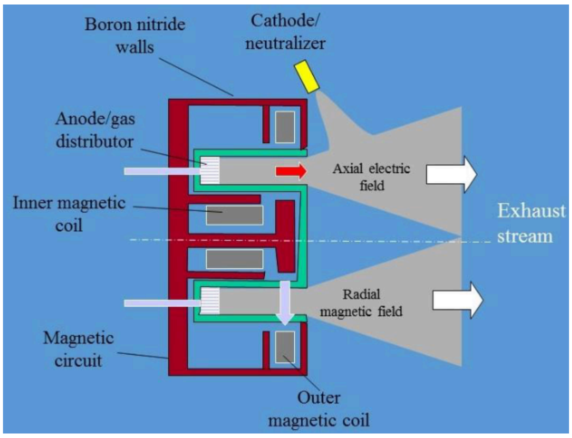

Figure 78: Schematic diagram of a Hall effect thruster.

11.3. Electric Propulsion Performance

Recall **Eq. 7**, **Eq. 8** and **Eq. 9** as well as **Figure 6** from lecture 2. These equations and figure have the following key takeaways:

- Electric propulsion exhaust velocity c and thrust F are **inversely proportional** to one another. A higher thrust means a lower exhaust velocity and performance and vice versa.
- Power input as well as power plant mass are **directly proportional** to thrust and acceleration. A higher thrust directly means a higher power input.
- In terms of values of the specific power plant mass:
  - $\alpha = 200 kg/kW$ for a RTG
  - $\alpha = 20 kg/kW$ for a solar panel
  - $\alpha = 2 kg/kW$ for a nuclear reactor (note that the mass will have to be very big though.)

Note that the performance of the 7 different electrical propulsion systems mentioned above is shown in **Table 13**.

Type	Thrust Range (mN)	I_{sp} Range (s)	Thruster Efficiency	P_{in} Range (W)
Electrothermal Propulsion Systems				
Resistojet	200 - 300	200 - 350	65 - 90	50 - 1000
Arcjet	200 - 1000	400 - 1000	30 - 50	900 - 2200
Electrostatic Propulsion Systems				
Ion Thruster	0.01 - 500	1500 - 8000	60 - 80	100 - 4300
Electrospray	0.001 - 1	300 - 6000	15 - 70	1 - 50
Electromagnetic Propulsion Systems				
PPT	0.05 - 1	600 - 2000	≈ 10	50 - 500
MPD thruster	0.001 - 2000	2000 - 5000	30 - 50	2000 - 100,000
Misc Electrical Propulsion Systems				
Hall Thruster	0.01 - 2000	1500 - 3500	20 - 60	100 - 100,000

Table 13: Comparative performance of different electrical propulsion systems.

11.4. Why Electric Propulsion ?

Electric propulsion systems are the dominant form of in-space propulsion, to understand why consider the rearranged form of the rocket equation shown in **Eq. 51**.

$$\frac{M_0}{M_f} = \exp\left(\frac{\Delta V}{I_{sp} g_0}\right) = \exp\left(\frac{\Delta V}{c}\right) \quad \longrightarrow \quad M_p = M_f \left(\exp\left(\frac{\Delta V}{c}\right) - 1\right) \tag{51}$$

Now consider an asteroid rendezvous mission with the following requirements:

- $M_{\text{Payload}} = 500kg$
- $c_{\text{Chemical}} = 3km/s$
- $\Delta V = 5km/s$
- $c_{\text{Electric}} = 30km/s$

For a chemical thruster, $M_p \approx 2000kg$ whereas for a electric thruster the $M_p \approx 90kg$. The downside here is the long burn time of electrical compared with chemical due to the very low thrust.

11.5. Uses of Electric Propulsion

Electric thrusters have seen wide spread use in space applications for both primary and secondary propulsion systems. These are:

- Primary propulsion systems
  - Interplanetary exploration.
  - Drag compensation in LEO.
  - Orbit raising.
  - Formation flying.
- Secondary Propulsion system
  - N-S station keeping.
  - E-W station keeping.

12. Lecture 12

12.1. History of Electric Propulsion

Some key points in the development of electric propulsion, from the initial development of EP to their widespread use, is shown in the timeline below:

- **20 July 1964** — SERT-1: First flight of an ion thruster
- **15 August 1991** — USSR Meteor-3: First in-space test of a Hall Effect Thruster.
- **24 October 1998** — NASA Deep Space 1 launch (first ion thruster on a science mission)
- **9 May 2003** — Hayabusa launch to asteroid Itokawa
- **13 June 2010** — Hayabusa sample return capsule to Earth
- **20 October 2018** — BepiColombo launch using UK T6 ion thruster
- **24 May 2019** — First SpaceX Starlink satellites launch (v0.9 batch)
- **13 October 2023** — NASA Psyche mission launch to asteroid Psyche
- **Mid-2025 (launch window)** — Lunar Gateway PPE + HALO first modules launch window

Note that there is a large gap between the first use of ion thruster and the first actual use on a mission, this was probably due to the following factors:

- **Lack of power production** (poor solar panel efficiency) on spacecraft.
- **Toxic propellants** that were chosen for the initial thrusters (mercury, cesium) and lack of safe propellants at the time (Xenon, Krypton).
- **Low number of launches**, due to this safe propellent options were prioritized.

12.2. Use of EP in Spacecraft

The number of satellites has grown incredibly over the l,ast few decades, going from a few hundred to over 9000 (inflated due to constellations). A graph of the cumulative number os satellites is shown in **Figure 79**. A large majority of these satellites utilize electric propulsion.

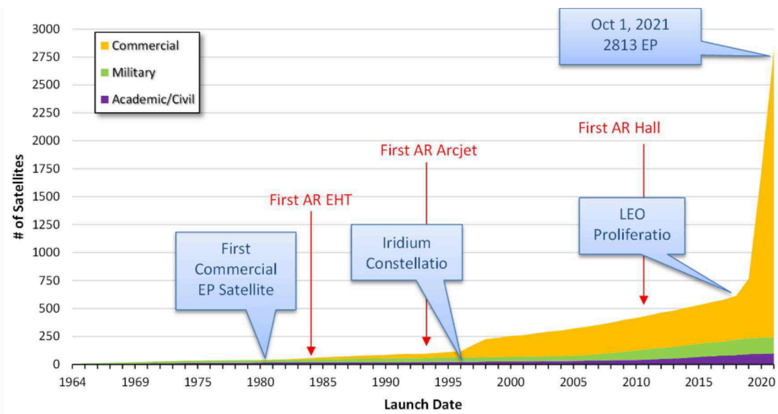

Figure 79: Cumulative number of satellites from 1964 - 2020.

12.3. EP Use-cases and Requirements

12.3.1. GEO Orbit Raising

For satellites which end up in a GEO, they are first inserted into a highly elliptical GTO (geostationary transfer orbit). From this an electric thruster is used to circularize the orbit and to then maintain the orbit (station keeping) over the lifetime of the mission. The key requirements of this mission type are shown below:

- **Thrust to power** defined by:
  - Time to do orbit transfer (current max is 6 months).
  - Power available per unit mass of satellite.
  - Due to these requirements, **30 - 70 mN/kW** is viewed as an acceptable value.
- The **power available** is defined by the available power on satellite, typically:
  - 1.5 tonne satellite: ~ 5 kW available.
  - 3 tonne satellite: ~ 10 kW available.
  - 6 tonne satellite: ~ 20 kW available.
- The **thruster lifetime** is based:
  - Transfer time: ~ 5000 hours
  - Station lifetime: 5000 - 10,000 hours.

On top of these requirements the $I_{sp} \approx 1000s$ for a good thruster.

12.3.2. LEO Orbit Raising

For many constellations as well as many other satellites, they are first dropped off in a LEO ($\approx 400km$) and need to then be raised to a higher LEO or even a MEO ($\approx 600 - 2000km$). Beyond this, some satellites also require some addition thrust for station keeping. The key requirements of this mission type are shown below: Requirements;

- **Thrust to power** defined by:
  - Time to do orbit transfer (current max is 1 year).
  - Due to this requirements, **40 - 60 mN/kW** is viewed as an acceptable value.
- The **power available** is defined by the available power on satellite, typically:
  - 200 kg satellite: ~ 500 W available.
  - 1.5 tonne satellite: ~ 5 kW available.
- The **thruster lifetime** is based:
  - Transfer time: ~ 10,000 hours
  - Station lifetime: dependant on satellite and mission.

On top of these requirements the $I_{sp} \approx 1000s$ for a good thruster.

12.3.3. Applicable Thrusters for Orbit Raising

Given the requirements for LEO and GEO rasing, there only exists a few electric thruster which can work in this regime. Consider **Figure 80**, the highlighted envelope shows the requirements for LEO and GEO raising. In reality only GITs, HETs and DCT(HEMPT) can be used, which type of thrusters are used for orbit raising are shown in **Figure 81**. As can be seen, HETs and GITs are most commonly used.

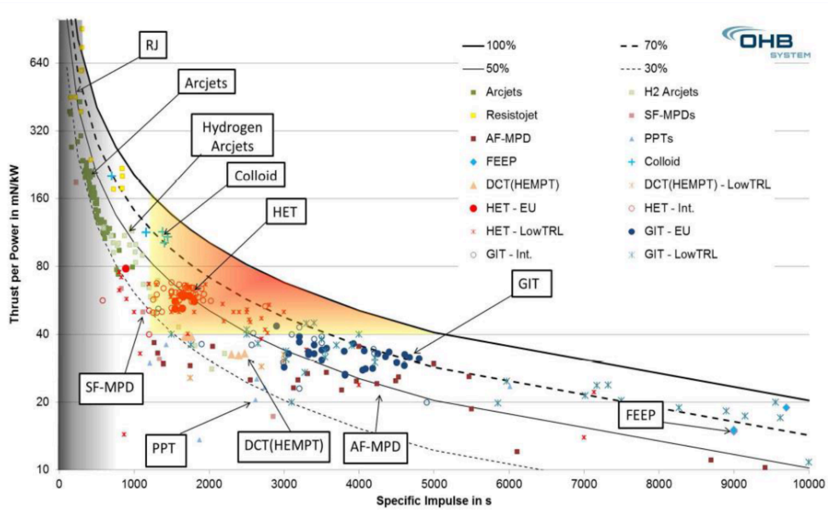

Figure 80: Plot of thrust per power against impulse for different electric thrusters, including low TRL and envelope for orbit raising.

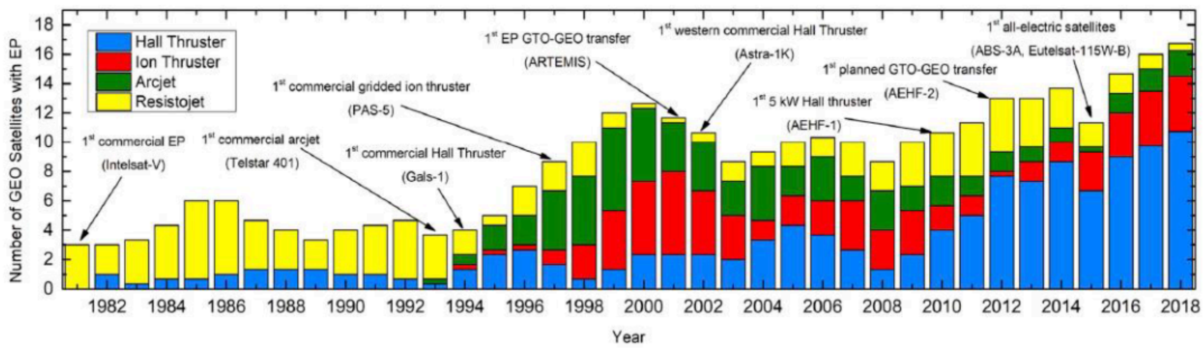

Figure 81: Plot showing which electric thrusters are used for orbit raising over time.

12.3.4. LEO and GEO Station Keeping

Many satellites require thrusters to maintain their orbit overtime. This equates to roughly **45 minutes of burning per day**. The requirements for these thrusters are different from orbit raising and are shown below:

- **Thrust to power** defined by:
  - Manoeuver time.
  - Required thrust to power is low as the thruster operation does not interfere with the satellite operation.
  - Thus specific impulse can be maximized.
  - Due to this requirements, **30 - 200 mN/kW** is viewed as an acceptable value.

- The **power available** is defined by the available power on satellite, typically:
  - Only limited power available as thruster must operate during payload operation.
  - Therefore power is supplied by either increasing solar array area or switching off of payload.
  - 1.5 tonne satellite: ~ 3 kW available.

- The **thruster lifetime** is based:
  - Dependent on thrust, mission, etc (~ 5,000 - 10,000h)

On top of these requirements the I_{sp} requirement is a bit lower than orbit raising.

12.3.5. Applicable Thrusters for Station Keeping

As the requirements for station keeping are more lax than the ones for orbit rasing, there are more available thrusters, the envelope defined by the requirements in the previous section is imposed in **Figure 82**.

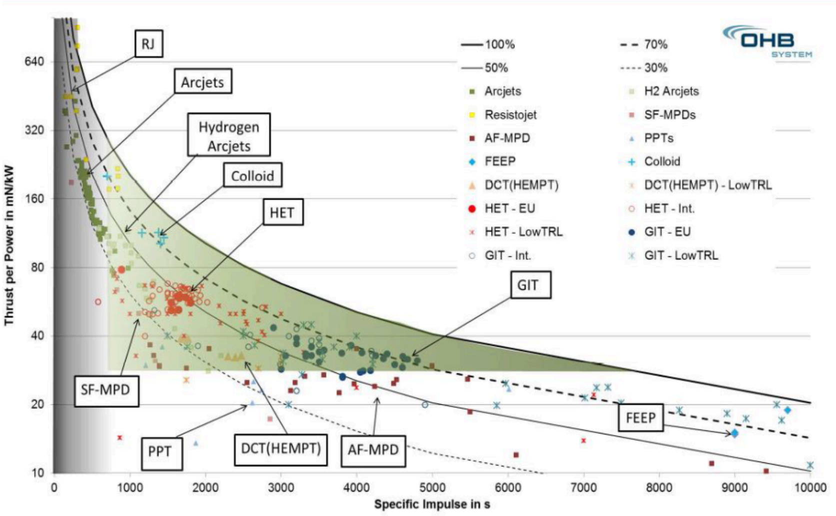

Figure 82: Plot of thrust per power against impulse for different electric thrusters, including low TRL and envelope for station keeping.

As is shown in **Figure 82**, some electrothermal propulsion methods become viable as well as some options augmented with hydrazine.

12.3.6. Interplanetary Missions

Interplanetary missions require a very large ΔV and so the main focus for the thruster is to have a very high I_{sp}. The full list of requirements for an interplanetary mission are shown below:

- **Thrust to power** defined by:
  - As the mission time is not a priority, the thrust to power is low meaning the mission time is very long (multiple years).
  - Due to this requirements, $>$ **20 mN/kW** is viewed as an acceptable value.
- The **power available** is defined by the available power on satellite, typically:
  - Defined by the final mission scenario.
  - Close to Earth, large power levels are available, further away lower power levels are available.
  - Only limited power available as thruster must operate during payload operation.
  - Therefore power is supplied by either increasing solar array area or switching off of payload.
  - 1.5 tonne satellite: ~ 3 kW available.
- The **thruster lifetime** is based:
  - Dependent on transfer time, typically ~ 40,000 - 80,000h.

On top of these requirements the I_{sp} requirement is very high ($I_{sp} \gg 3000s$).

12.3.7. Applicable Thrusters for Interplanetary Missions

Due to their high I_{sp} and low thrust-to-power requirement, the envelope for available thrusters is pushed to the right. This means that only GITs and some high performance HETs can be used, this is shown in **Figure 83**.

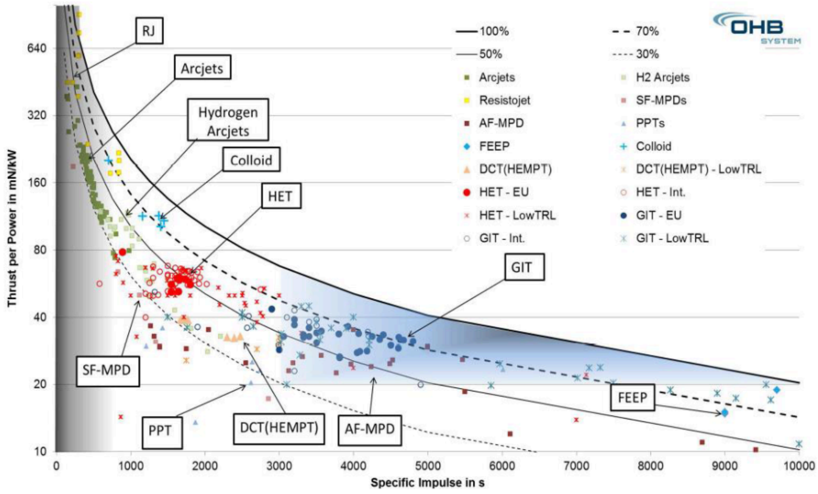

Figure 83: Plot of thrust per power against impulse for different electric thrusters, including low TRL and envelope for interplanetary missions.

12.4. Derivation of an Electric Thruster Rocket Equation

Consider a simple spacecraft consisting of the following subsections which all have the following masses (assuming spacecraft structural mass to be negligible):

- $\boldsymbol{M_{Pay}}$: Mass of the payload (kg)
- $\boldsymbol{M_{Pow}}$: Mass of the power plant (kg)
- $\boldsymbol{M_P}$: Mass of the propellent (kg)

With these three sections being connected to a thruster. The initial mass of the spacecraft is therefore defined by **Eq. 52**.

$$M_0 = M_{Pay} + M_{Pow} + M_P \tag{52}$$

An expression for the mass of the power plant can be defined by substituting the equations defined in **Eq. 53** into **Eq. 52**.

$$M_P = \dot{m}t_b \qquad \eta_T = \frac{\dot{m}c^2}{2P_{in}} \qquad P_{in} = \frac{M_{Pow}}{\alpha} \tag{53}$$

The equation for the power plant mass is therefore defined in **Eq. 54**, where v_c is the characteristic velocity, not to be confused with c^*.

$$M_{Pow} = \frac{M_0 - M_{pay}}{1 + \left(\frac{2\eta_T t_b}{\alpha c^2}\right)} = \frac{M_0 - M_{pay}}{1 + \frac{v_c^2}{c^2}} \qquad v_c = \sqrt{\frac{2\eta_T t_b}{\alpha}} \tag{54}$$

Utilizing **Eq. 54**, rearranging it and substituting in to the rocket equation yields **Eq. 55**.

$$\Delta V = c \ln \left(\frac{1 + \frac{v_c^2}{c^2}}{\frac{M_{Pow}}{M_0} + \frac{v_c^2}{c^2}} \right) \tag{55}$$

As **Eq. 55** is an unintuitive equation, it has been plotted out with ΔV against increasing exhaust velocities in **Figure 84**.

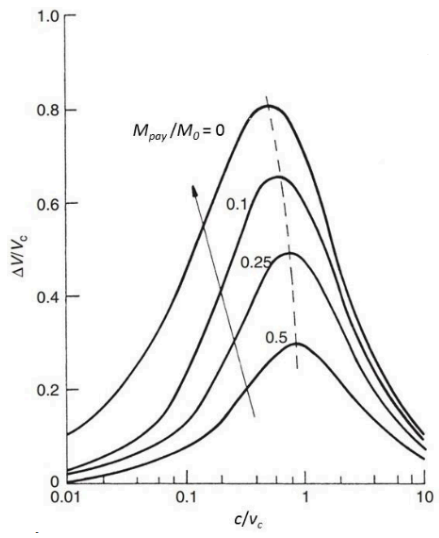

Figure 84: Plot of normalized ΔV against normalized exhaust velocities.

Note that as the exhaust velocity increases, the ΔV does not continually increase, instead it starts to eventually decrease and this is because after a point the mass of the power plant needed to produce the power to accelerate the exhaust outweighs any ΔV gain. Another way of thinking about this is that $M_{Pow} \propto I_{sp}$ and $M_P \propto 1/I_{sp}$, meaning that there is an optimal mass of the spacecraft. **Figure 84** also has the following takeaways:

- For high I_{sp}s, if the system is operating at conditions to maximize performance, then t_b will be high.
- For an optimum burn time $t_{b_{\text{Max}}} \approx (\Delta V)^2$
- An optimum I_{sp} is roughly equal to the required change in velocity, $I_{\text{sp}_{\text{Optimum}}} \approx \Delta V$

13. Lecture 13

START OF WEEK 7

13.1. Introduction to Plasma

A useful definition for plasma is a **a quasineutral gas of charged and neutral particles which exhibits collective behavior**. A plasma is formed when atoms gain enough energy (through heating or through other means) to be stripped of their electrons. As the plasma is a "soup" of ions, electrons and particles, the plasma as a whole will be **quasineutral**. The plasma itself will exhibit a **collective behavior** as ions and electrons will all experience electrostatic forces between one another.

13.2. Debye Length

One Fundamental property of a plasma is the **Debye length** shown in **Eq. 56**.

$$\lambda_D = \sqrt{\frac{\varepsilon_0 k T_e}{n e^2}} \tag{56}$$

Where:

- $\boldsymbol{\varepsilon_0}$: Permittivity of free space $= 8.85 \times 10^{-12} m^3 kg^{-1} s^4 A^2$
- $\boldsymbol{k}$: Boltzmann's constant $= 1.38 \times \times 10^{-23} JK^{-1}$
- $\boldsymbol{e}$: Electron charge $= 1.6 \times 10^{-19} C$
- $\boldsymbol{T_e}$: Electron temperature (K)
- $\boldsymbol{n}$: Plasma density (Number of Particles/m^3)

Note that as the plasma is quasineutral, the density of ions and electrons must be the same. Further note that the electron temperature will be higher than the ion and particle temperature as the electrons are able to reach higher temperatures. To understand what the Debye length is, consider the scenario shown in **Figure 85**.

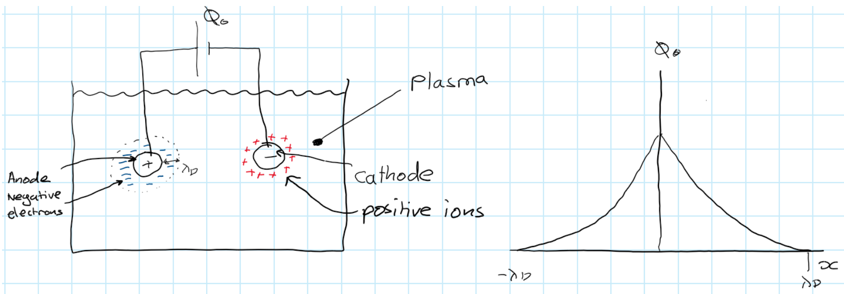

Figure 85: Figure of potential applied across a plasma with a plot of teh potential difference against the distance away from the anode/cathode.

As a potential is applied across a plasma, the ions and electrons form a sheath around the cathode and anode respectively. This acts to neutralize the effect of the potential difference applied to the plasma. One key point is that the **debye length must be smaller than the size of the container** for the substance within it to be considered a plasma.

14. Lecture 14

14.1. Charged Particle Motion in Magnetic Fields

A charged particle subjected to a constant magnetic field will undergo circular motion, this is because the force on teh charged particle will be centripetal towards the center of rotation (called the **guiding centre**). The force on a charged particle is given by the Lorenz force shown in **Eq. 57**.

$$\vec{F} = q\vec{v} \times \vec{B} \tag{57}$$

Where:

- $\vec{\boldsymbol{F}}$: Force vector (N)
- $\boldsymbol{q}$: Magnitude of charge of the particle (C)
- $\vec{\boldsymbol{v}}$: velocity vector (m/s)
- $\vec{\boldsymbol{B}}$: Force vector (T)

The angular velocity at which the charged particle rotates with is given by the **cyclotron frequency** and is shown in **Eq. 58**.

$$\omega_c = \frac{q\vec{B}}{m} \tag{58}$$

Where:
- $\boldsymbol{\omega_c}$: Cyclotron frequency (rad/s)
- $\boldsymbol{m}$: Particle mass (kg)

The radius of the circle that the charged particle rotates through is called the **Larmor radius** and is shown in **Eq. 59**.

$$r_L = \frac{v_\perp}{\omega_c} = \frac{mv_\perp}{q\vec{B}} \tag{59}$$

Where:
- $\boldsymbol{r_L}$: Larmor radius (m)
- $\boldsymbol{v_\perp}$: Perpendicular velocity (m/s)

14.2. Charged Particle Motion in Electric Fields

A charge particle within an electric field will experience a constant force given a uniform electric field strength. The force on a charged particle in an electric field is given by the Lorenz force shown in **Eq. 60**.

$$\vec{F} = \vec{E}q \tag{60}$$

Where $\vec{\boldsymbol{E}}$ is the electric field strength with units N/C.

14.3. Charged Particle Motion in Magnetic and Electric Fields

In a space where there is an electric field and a magnetic field perpendicular rto one another, a charged particle that enters that field will travel in a spiral pattern, this is show in **Figure 86**.

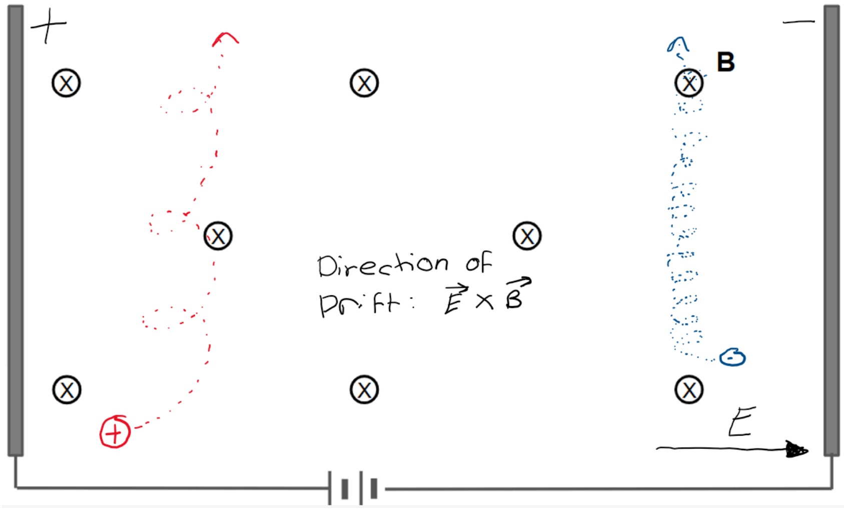

Figure 86: Path taken by an ion and electron in a magnetic and electric field.

Note that in **Figure 86**, regardless of the polarity of the magnet or direction of the electric field, an electron and positive ion will drift in the same direction, the only difference would be how tight their radii were. Note that the direction of the drift is obtained by $\vec{E} \times \vec{B}$. Note that this motion is similar to a charged particle in a varying magnetic field, shown in **Figure 87**.

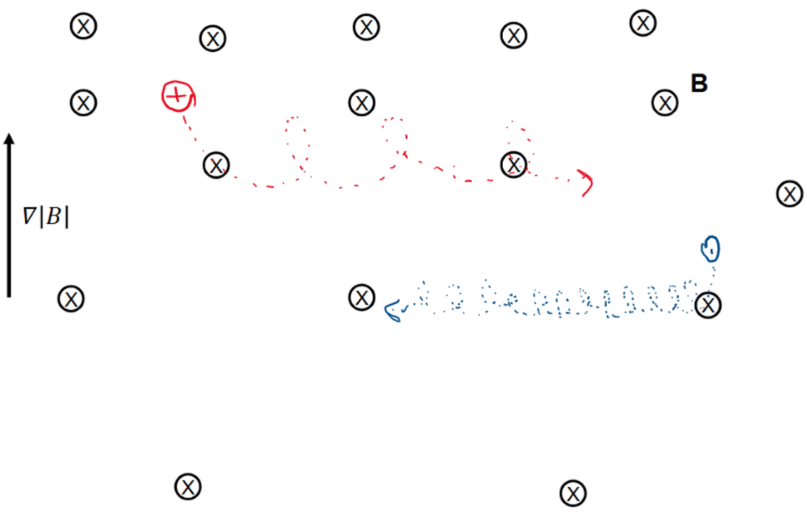

Figure 87: Path taken by an ion and electron in a non-constant magnetic.

Note that in **Figure 87**, whether the particle is an ion or electron dictates the direction it will drift in.

14.4. Magnetic Mirroring

Consider a charged particle moving in a spiral along a magnetic field line. If the magnetic field density increases, then the particle will start to spiral faster ($v_\perp \uparrow$) and the Larmor radius will tighten, this is show in **Figure 88**.

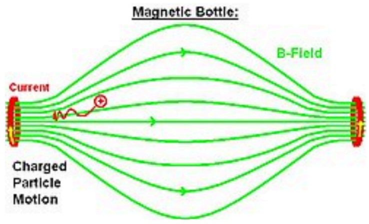

Figure 88: Magnetic mirroring.

As the perpendicular speed increases, there must be a decrease in the parallel speed to conserve energy, this means that eventually the parallel velocity goes to zero and inverts, causing magnetic mirroring. This can also be seen in the magnetic moment of a gyrating particle equation shown in **Eq. 61**.

$$\mu = \frac{1/2 m v_\perp^2}{B} = const \tag{61}$$

As μ must remain constant and B increases, $v_\perp$ decreases in proportion, increasing the speed at which the particle rotates.

14.5. Working Principle Behind Hall Effect Thrusters

Hall Effect Thrusters (HETs) utilize many of the physical concepts mentioned previously to ionize and accelerate a gas. An image showing the major components of a HET is shown in **Figure 89**.

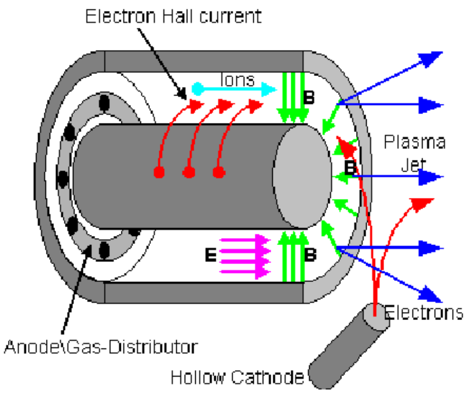

Figure 89: Basic componenets of a Hall Effect thruster.

To better understand the working principle behind a HET, we will consider the lifecycle of an electron, this is shown below:

1. Electrons are produced in the hollow cathode (some of the produced electrons ionize the ionized plasma jet).
2. Electrons are attracted towards the anode at the bottom of the annular channel.

3. Electrons see a strong magnetic force at the mouth of the annular channel where they start to rapidly spiral around (this creates a strong negative charge at the mouth accelerating ions).
4. The electrons are still attracted to teh positive anode and very slowly drift down to the anode.
5. Closer to the anode, neutrals are ionized, producing ions which are accelerated out.
6. Electrons collide with the anode completing the circuit.

In reality the movement of electrons is more complex with wall collisions and magnetic mirroring occurring. Furthermore, it is still not understood why electrons eventually break away from the magnetic confinement area. The real motion of the particles is show in **Figure 90**. Also shown is a plot of electric field strength and magnetic field strength, it can be sean that at the mouth where there is the strongest magnetic field, is where the strongest electric field is due to the magnetic confinement.

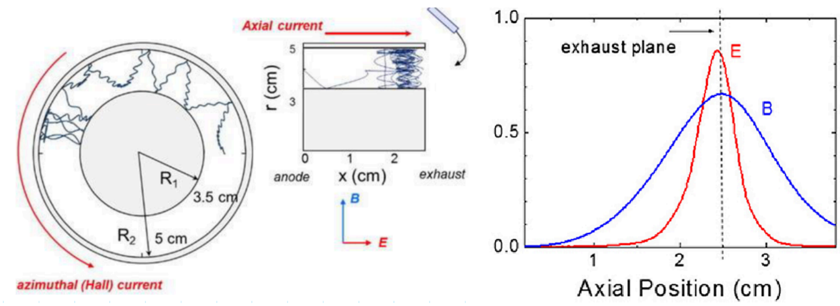

Figure 90: Simulated movement of electrons in a hall effect thruster.

14.6. HET Performance and Improvement Areas

HETs sit at almost a goldilocks zone of performance, having much better performance then chemical or electrothermal thrusters whilst having higher thrust than GITs. A table comparing the performance of GITs to HETs is shown in **Table 14**

Type,	Thrust Range (mN)	Isp Range (s)	Thruster Efficiency	Input Power Range (W)
Gridded Ion Thruster	0.1 - 300	1500 - 5000	60 - 80	400 - 4300
Hall Thruster	5 - 2000	1000 - 2000	30 - 60	1000 - 50,000

Table 14: HET vs GIT performance.

However HETs do have drawbacks when compared to other electrical thrusters, some of the main drawbacks are:

- **Large beam divergence** (30 - 40 degrees), this is caused by non-uniform electric and magnetic fields as well as the rotation that that the ions experience when in the magnetic field. This **reduces thrust**.
- **Electromagnetic interference** which is caused by plasma oscillations. This is due to the predator prey relationship between electrons, neutrons and ions.
- **Poor lifetime**, however this may be fixed through magnetic shielding.

14.7. HET Lifetime and Magnetic Shielding

HETs struggle with performance over their lifetime due to the magnetic confinement eroding teh material near the mouth, this effect is shown in **Figure 91**.

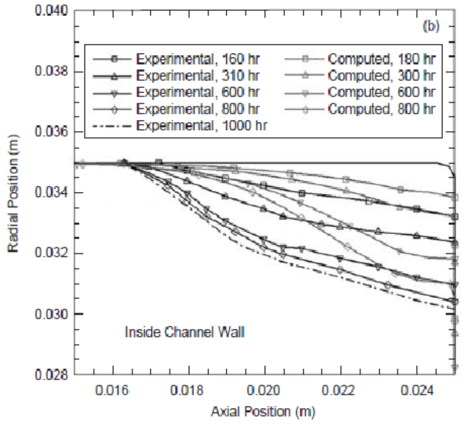

Figure 91: Erosion rate of HET near at the mouth.

One new method of mitigating this is by using a shielded magnet, this has the effect of moving the magnetic confinement region away from the walls, decreasing the erosion rate. A figure of magnetic shielding as well as the erosion rate with and without it (red and dashed red line) are shown in **Figure 92**.

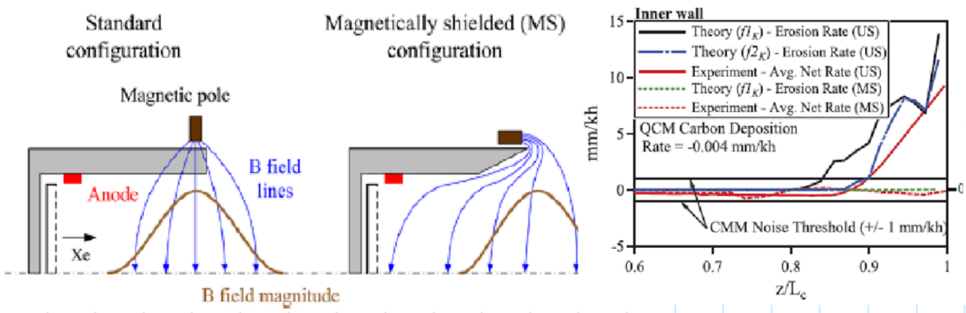

Figure 92: Magnetic shielding implemented on a HEt with teh new and old erosion rates.

14.8. HET Propellants

Xenon and Krypton are mostly used as HEt propellants due to their high atomic weight and relative ease of obtaining. Various different propellants are shown in **Figure 93**.

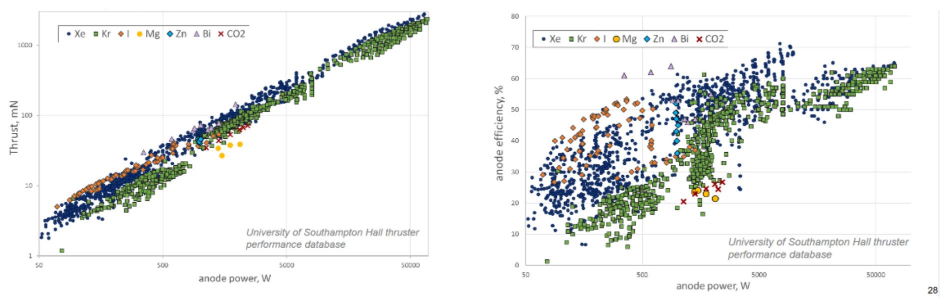

Figure 93: HET propellent performance